Construction and Building Materials 267 (2021) 120849

Contents lists available at ScienceDirect

Construction and Building Materials

journal homepage: www.elsevier.com/locate/conbuildmat

Development of sandwich panels for multi-functional strengthening of RC buildings: Characterization of constituent materials and shear interaction of panel assemblies

Christoph de Sousa [a,*], Joaquim A.O. Barros [a], João Ramôa Correia [b], Tiago D.S. Valente [c]

[a] ISISE – Institute for Sustainability and Innovation in Structural Engineering, University of Minho, School of Engineering, Department of Civil Engineering, Campus de Azurém, 4800-058 Guimarães, Portugal
[b] CERIS – Civil Engineering Research and Innovation for Sustainability, Instituto Superior Técnico, Universidade de Lisboa, Avenida Rovisco Pais, 1049-001 Lisboa, Portugal
[c] CiviTest, Rua da Indústria, n.°144, Parque Industrial de Jesufrei, 4770-160 Vila Nova de Famalicão, Portugal

HIGHLIGHTS

- Sandwich panel concept for structural and thermal retrofit of existing RC-buildings;
- Extensive laboratory characterization of the panel's individual components;
- Use of recycled steel fibres as discrete reinforcement of thin concrete wythes;
- Pullout tests for selection of insulation layer and GFRP connectors;
- Numerical simulation of pullout test using 3D surface interface finite elements.

ARTICLE INFO

Article history:
Received 9 January 2020
Received in revised form 25 August 2020
Accepted 5 September 2020
Available online 9 November 2020

Keywords:
Rehabilitation of RC-buildings
Building facades
Sandwich panel
Precast concrete
Recycled steel fibres
GFRP connectors
Polystyrene
Pushout tests
Pullout tests
Finite element method

ABSTRACT

This paper presents an experimental and numerical study aiming at the development of a sustainable and multifunctional composite sandwich panel for the rehabilitation of reinforced concrete (RC) buildings from the 1960s to the mid-1980s. The sandwich panel, which was designed for the structural, thermal and acoustic refurbishment of building facades, comprises three main components: (i) thin outer layers of Recycled Steel Fibre Reinforced micro–Concrete (RSFRC) that fulfil the strength, ductility and durability requirements of the panel; (ii) a lightweight core made of polystyrene that provides thermal insulation; and (iii) internally distributed glass fibre reinforced polymer (GFRP) connectors that join the different layers of the panel, providing an adequate structural behaviour to the composite system. The mechanical characterization tests highlighted the viability of using RSFRC for the production of structural sandwich facade panels, as relatively high post-cracking tensile capacity was obtained for thin RSFRC layers. Pushout and pullout tests were carried out on intermediate-scale specimens representative of the sandwich panel solution for assessing the overall composite behaviour of the sandwich panels and analysing the influence of the type of core insulation layer (expanded/extruded polystyrene cores, with different surface finishing), of the anchoring conditions (25 and 35 mm of embedment depth) and diameter of the GFRP connectors (8 and 12 mm). These tests showed that the structural GFRP connectors with diameters of 8 and 12 mm are able to ensure shear load transfer between RSFRC layers, exhibiting better composite behaviour when combined with anchorage depths of 25 and 35 mm, respectively. The numerical part of this study aimed at modelling the failure mechanisms observed at the interface between RSFRC and polystyrene, showing good agreement between experimental and numerical results, with important conclusions being drawn regarding cohesion and friction angle between these materials.

1. Introduction

During the past decade, the main interests of the construction industry and research community regarding the retrofit of existing housing stock have been focused on three different areas: (i) struc-

* Corresponding author.
E-mail address: christophdesousa@civil.uminho.pt (C. de Sousa).

https://doi.org/10.1016/j.conbuildmat.2020.120849
0950-0618/

tural rehabilitation, in view of the safety of buildings and protection of their inhabitants (*e.g.*, buildings that exhibit structural vulnerabilities under seismic actions) [1–7]; (ii) energetic refurbishment [8–10], mostly due to the targets defined by governmental authorities and international organizations regarding energy efficiency [11], indoor comfort in buildings, reduction of carbon emissions [12], and use of on-site renewable energy sources [13]; and (iii) use of sustainable resources in civil engineering structures in view of society's environmental and economic benefits [14–18]. In fact, the activities of rehabilitation and conservation of the built patrimony constitute very relevant issues for modern societies, not only due to the natural ageing and deterioration of civil engineering structures, but also because modern design codes involve higher requirements that a significant portion of existing buildings cannot cope with.

In this context, the research presented in this paper aims to address the above-mentioned challenges through the development of a multifunctional and sustainable precast concrete sandwich panel for the structural, thermal and acoustic (topic not covered in the present paper) rehabilitation of existing reinforced concrete (RC) frame buildings that were built in Portugal during the 1960-80s decades. Fig. 1 presents a 3D representation of the developed prototype, which comprises three main components: (i) thin outer layers made of recycled steel fibre reinforced micro-concrete (RSFRC); (ii) a lightweight core made of polystyrene; and (iii) internally distributed glass fibre reinforced polymer (GFRP) connectors (functional – F-GFRP – and structural – S-GFRP – connectors), which join the different layers of the panel. The objectives of the panel solution proposed in this study are three-fold: (i) to improve the structural, thermal and acoustic performance of the target buildings; (ii) to develop a sustainable sandwich system, through the incorporation of recycled steel fibres in the panels' wythes; and (iii) to guarantee an adequate composite action between the panels' components. The next paragraphs address each of the indicated objectives.

The building typology that was targeted for this research includes multi–storey RC structures; their structural configuration is based on foundations, columns, beams, slabs and central core walls, which are connected to each other forming RC moment-resisting frame structures. RC core wall systems were regularly adopted as the main lateral load resisting systems in highly seismic zones to provide lateral strength and stiffness for limiting the structural drift, especially for tall buildings [19]. However, since modern seismic design codes were introduced in Portugal only in 1983 [20], structural elements in this period were mostly designed for gravity loads, namely through simplified individual plane frame analysis, hence not addressing modern seismic design requirements. In this type of buildings, the moment resisting frames are typically arranged in one specific direction (see Fig. 2a) and linked to each other through edge beams and slabs that act as bracing members (as depicted in Fig. 2b), forming the final structural configuration presented in Fig. 2c, with inclusion of masonry infill walls.

The use of single-layer or double-layer masonry walls was a widespread solution adopted for the envelope walls. However, the introduction of thermal insulation systems into the cavity of double brick walls has only began in the 1980s and this practice only became typical in Portuguese building construction during the 1990s [21]; hence, a significant percentage of this type of buildings require thermal retrofit. These structural and thermal deficiencies are also significant and recurrent in the housing stock of other seismic-prone south Mediterranean European countries, such as Italy, south of France, Spain, Greece and Turkey, for which the proposed retrofit solution might also be applied.

Nowadays, waste management of used pneumatic tyres is still a major environmental challenge worldwide; both the reuse of tyres and the recovery of constituent materials are sustainable options for disposing of post-consumed tyres [22]. At the same time, in the field of civil engineering, due to a growing interest regarding innovative and recycled materials for sustainable building construction, research efforts have been made towards the incorporation in concrete of different by-products obtained from the recycling of waste tyres, namely granulated rubber [17,23] and steel fibres [18,22]. The addition of small fractions of recycled steel fibres (RSF) to the concrete during mixing is one example of such strategy, with research studies on this topic reporting favourable

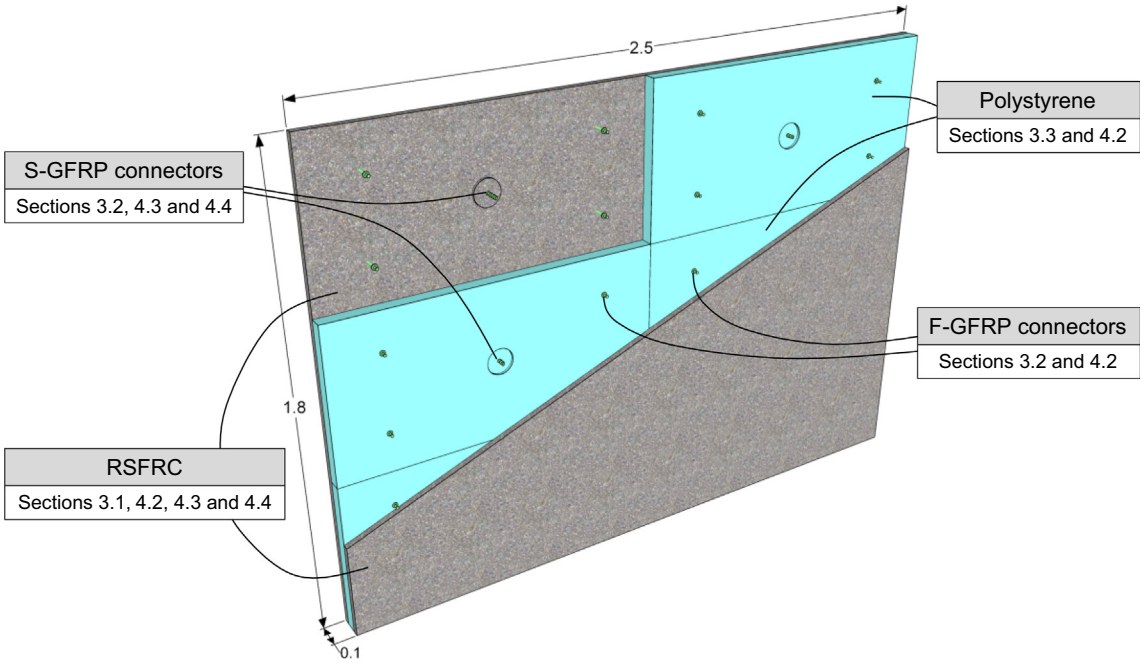

Fig. 1. 3D representation of the sandwich panel concept, with indication of the sections in which each component is addressed [dimensions in m].

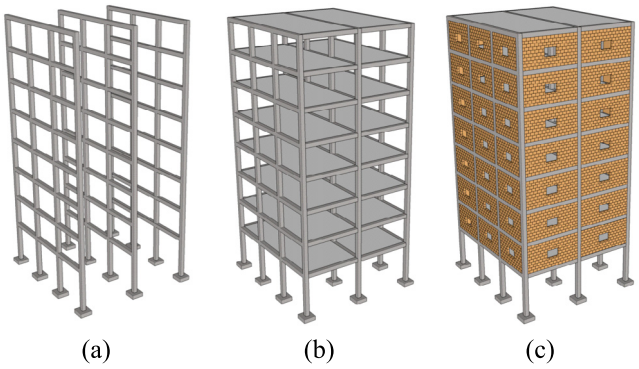

Fig. 2. Typical structural configuration of target buildings: (a) RC moment frames arranged in parallel; (b) RC frames with bracing members and slabs; (c) final RC structures, with masonry infill on envelope walls.

effects on concrete structures in terms of structural efficiency. In fact, it has been shown that such incorporation can decrease the brittleness of the concrete matrix in tension, enhancing its toughness and post-cracking resistance [24–27].

By using steel fibres resulting from the tyre recycling industry, instead of industrial steel fibres (ISF), as discrete reinforcement of the outer concrete layers of the sandwich panel (also referred to as *wythes*), significant environmental benefits can be retrieved, as was demonstrated by Frazão [28] in a life cycle assessment. From an eco-efficiency point of view, another relevant feature of the rehabilitation solution proposed is the thermal insulation enhancement provided to the facade and the consequent reduction of energy consumption.

Sandwich panels are often designed as multifunctional composite components due to their capacity to address various requirements, namely structural, thermal and acoustic. Such capacity stems partly from the insulation layer that separates the outer load-bearing layers. For insulated precast concrete sandwich panels, rigid foam insulation plates are frequently used, such as polystyrene plates, due to their lightweight and low thermal conductivity. More specifically, expanded polystyrene (EPS) and extruded polystyrene (XPS) are amongst the most common insulation materials. In terms of structural design, sandwich panels are usually categorized as fully, partially or non-composite, according to the degree of composite action between concrete wythes, which can be assessed by performing pushout tests designed to study the shear interaction between the referred wythes [29–37]. This shear interaction is known to be highly dependent on the connection between wythes, typically provided by shear connectors or solid concrete regions [37,38]. The available literature has shown that the insulation layer can also contribute to the panels' composite action depending on its mechanical and surface properties [29,39]. The relevance of this contribution depends mainly on the adhesion between the insulation and the surrounding concrete layers, which is addressed in the present research work.

This paper presents the first part of the experiments that were conducted towards the development of the sandwich panel described above (additional information can be found in Section 2). For this stage of the development process, the experiments included: (i) material characterization tests of the different individual components of the sandwich panel - external RSFRC layers, GFRP connectors and polystyrene core layer; and (ii) pushout and pullout tests on sandwich panel specimens subjected to shear loads. The former tests, described in Section 3, aim at collecting relevant information about the properties of the constituent materials. The latter experiments, described in Section 4, aim at defining (i) the insulation material to be adopted in the sandwich panel, taking into account the influence that different insulation typologies (in terms of material and surface finishing) have on the overall composite behaviour of the panel, and (ii) the structural GFRP connectors (type and spacing) distributed along the sandwich panel. Finally, Section 5 of this paper presents the numerical simulations conducted to model some of the complex failure mechanisms that were observed during the experimental findings, as well as to determine the cohesion and friction angle of the interfaces between the materials forming the panel, which are mobilized in the shear loading process.

2. Sandwich panel concept proposal

This Section provides a more detailed description of the sandwich panel concept, namely in terms of the underlying rehabilitation approach. An overall representation of the rehabilitation process, focused on the refurbishment of exterior walls and building facades, can be found in Fig. 3a. The intervention process to be conducted on the existing structure (Fig. 3b, detail 1) initiates with the removal/demolition of existing masonry envelope walls (Fig. 3b, detail 2), followed by the application of the sandwich panel (Fig. 3c, detail 3). The connection between the panel and the existing RC structural elements is ensured resorting to commercial anchoring systems (provided by *Hilti*, or equivalent system) and metallic angle profiles. The angle profiles (Fig. 3c, detail 6) are fixed to the beams and columns of the existing structural elements (contour of each envelope wall) prior to the application of the sandwich panel, using mechanical/expansion anchors (Fig. 3c, detail 4). The panel is then placed in its final position and fastened to the angle profiles using adhesive anchor bolts (Fig. 3c, detail 5).

This approach is based fundamentally on four principles: (i) the inner RSFRC layer acts as structural infill wall, to provide structural strengthening to the RC-frames against lateral loads; (ii) the insulation layer covers a wider area of the building envelope, including localized RC structural elements of the existing building; (iii) the outer RSFRC layer acts as protection layer for the building and can be connected to the adjacent facade panels to provide additional structural strengthening; and (iv) the GFRP connectors are the only structural components that link the inner to the outer RSFRC layers (Fig. 3c, detail 7), hence avoiding localized thermal bridges.

A potentially relevant aspect is the fire behaviour of the sandwich panel proposed herein – two main aspects are identified in this respect: (i) the fire reaction behaviour, due to the combustibility of the insulation layer (particular attention needs to be given to the detailing of joints and edges); and (ii) the reduction of composite action and the risk of delamination of the exterior RSFRC wythe, due to the softening of the GFRP connectors when exposed to elevated temperature (a redundant metallic anchoring system, connecting the exterior wythe to the RC structure may be necessary). Both these aspects, not covered in the present paper, require further specific investigations.

3. Material characterization

3.1. Recycled steel fibre reinforced micro-concrete (RSFRC)

The final composition of the RSFRC, which was developed specifically for the production of thin concrete layers to be adopted as wythes of precast sandwich panels, is presented in Table 1. Taking into account the adopted thickness for the concrete layers of the studied sandwich panel, defined as 25 mm, a nominal maximum aggregate size of 9 mm was adopted, therefore justifying the "micro-concrete" designation that was attributed to the concrete composition.

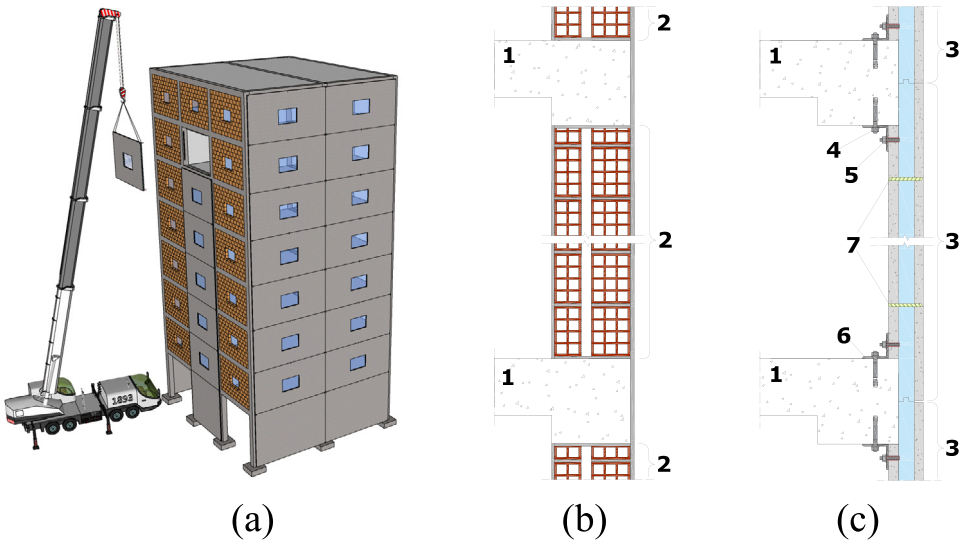

Fig. 3. Rehabilitation concept proposal: (a) 3D illustration of rehabilitation process; (b) original envelope walls (1 - existing structure; 2 - masonry envelope walls); (c) application of sandwich facade panels (3 - sandwich panel; 4 - mechanical anchor; 5 - adhesive anchor; 6 - angle profile; 7 - GFRP connectors).

Table 1
RSFRC mixture composition.

Component	Content [kg/m^3]
Cement (CEM I 42.5R)	400.0
Fly ash	200.0
Water	173.0
Crushed granite (9 mm)	597.2
River sand (4 mm)	734.7
Fine sand (0.6 mm)	147.5
Superplasticiser (BASF SKY 617)	7.2
Recycled steel fibres	70.0

The RSF used for this research were obtained through a commonly used tyre recycling technique that is applied to post-consumed truck tires, which combines mechanical shredding and granulation. Further processing of the RSF through an electromagnetic extraction system ensures the separation of the steel fibres from the rubber matrix. The fibres obtained from this process have irregular diameters, lengths and shapes. The average values that characterize the fibres used in this research, obtained from a thorough geometric and mechanical characterization study involving a representative sample of approximately 60,000 fibres [40], are as follows: length (l_f) of 23 mm, diameter (d_f) of 0.22 mm, aspect ratio (l_f / d_f) of 100, elastic modulus of 200 GPa and tensile strength of 2570 MPa. An RSF volume content of 0.89% (70 kg/m^3 per concrete m^3) was added to the concrete mixture composition, constituting the only steel reinforcement of the concrete layers (*i.e.*, no conventional mesh or rebar steel reinforcement was adopted).

The modulus of elasticity and compressive strength of the RSFRC were assessed at the age of 28 days by testing cylinders with 150 mm of diameter and 300 mm of height, according to standards EN 12390-13 [41] and EN 12390-3 [42], respectively. The average values obtained for the modulus of elasticity and compressive strength were, respectively, 27.5 GPa (coefficient of variation, CoV, equal to 2.5%) and 50.3 MPa (CoV = 7.8%).

The post-cracking behaviour of the RSFRC was assessed by direct tensile tests on notched dog-bone shaped specimens, also at the age of 28 days. The test setup, depicted in Fig. 4a, includes a servo-controlled direct tensile testing machine with an actuator and load cell of 50 kN capacity, and two ribbed grips that secured the specimen on both ends. Additionally, four inductive proximity sensors [43] were installed at the lateral, front and back faces of the specimens, near the notch tip, in order to measure the crack mouth opening displacement (CMOD), which was determined by the average value of the displacements registered by the referred sensors. The geometric configuration of the specimens, which had 30 mm of thickness, is presented in Fig. 4b. Notched specimens were adopted since a tensile strain softening behaviour was expected for this composite material, therefore the notch and the monitoring systems were able to determine the fracture mode I parameters for the developed RSFRC. The tests were performed by imposing a displacement rate of 0.1 mm/min to the top grip of the equipment. A slow displacement rate was adopted to enable observing and capturing as accurately as possible the evolution of the CMOD, which was recorded continuously at a rate of 4 Hz. Fig. 4c presents the envelope (with representation of confidence interval, corresponding to a confidence level equal to 95%) and corresponding average tensile stress *vs.* CMOD relationships obtained in these tests (8 specimens were tested, in total). At crack initiation and at peak load, average tensile stresses of 3.7 MPa (CoV = 8.5%) and 3.9 MPa (CoV = 6.5%) were obtained, respectively. The post-cracking behaviour is characterized by residual tensile strengths of 3.3 MPa (CoV = 10.3%) and 1.6 MPa (CoV = 30.3%) at CMOD = 0.5 mm and CMOD = 2.5 mm, respectively, being these last two residual strength values used to establish the stress-crack width constitutive relationship for the design analysis at service and ultimate limit states according to the Model Code 2010 [44]. The obtained post-cracking ductility assumes particular importance for this material in light of its incorporation in seismic applications, as it can have a relevant contribution for increasing energy dissipation during a seismic event.

3.2. GFRP connectors

Two types of GFRP connectors were used during the experimental program. Both GFRP connectors were specifically designed for the production of sandwich panels in the precast concrete industry, namely to provide connection between outer concrete wythes and an inner insulation layer (for typical concrete/polystyrene/concrete sandwich panel configurations). Taking into account the thickness of the sandwich panel under development in the scope of this research project (*cf.* Fig. 1), the adopted connectors had total length

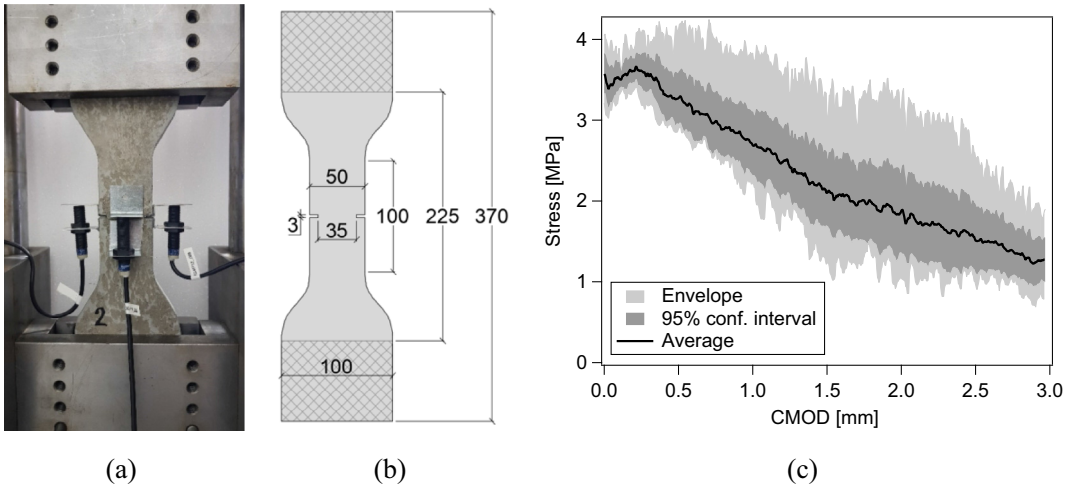

Fig. 4. Evaluation of tensile properties of RSFRC: (a) Test setup; (b) Specimen geometry [dimensions in mm]; (c) Load *vs.* CMOD curves.

of 100 mm, compatible with a sandwich panel solution encompassing external concrete wythes of 25 mm of thickness each, and a 50 mm thick core insulation layer (see cross-sectional dimensions in Fig. 5a). The first connector, hereby designated as "F-GFRP", is a connector of functional nature that allows for higher quality control of the sandwich panels during the casting process (see Fig. 5a, left-hand side). In fact, the connector has a protruding thicker section in the upper concrete/insulation layers' transition, which acts as a gauge for an easier control of the position of the insulation layer and, consequently, of the thickness of the RSFRC layers. The second connector, designated as "S-GFRP", is a structural connector, which consists of ribbed glass fibre reinforcing bars with the ends inclined at 30° (*cf.* Fig. 5a, right-hand side).

Uniaxial tensile tests on GFRP connectors were performed on two universal test machines (UTM), with load capacities of 1000 kN (F-GFRP, Fig. 5b) and 250 kN (S-GFRP). The axial stress *vs.* strain curves obtained are shown in Fig. 5c According to the data provided by the suppliers, the F-GFRP and S-GFRP connectors have tensile modulus of 10.1 GPa and 60.0 GPa, respectively, and tensile strength of 91 MPa and 1000 MPa, respectively. The average tensile modulus and tensile strength measured in the tests were 10.4 GPa (CoV = 12.2%) and 96 MPa (CoV = 1.3%) for the F-GFRP connectors, and 58.4 GPa (CoV = 2.7%) and 1320 MPa (CoV = 12.5%) for the S-GFRP connectors (see Fig. 5c), respectively. These results are in agreement with the data provided by the suppliers of the F-GFRP [45] and S-GFRP connectors [46]. Obtained properties show that the S-GFRP connectors present higher tensile strength than steel rebars and can therefore be regarded as an adequate solution in light of the multidisciplinary nature of the objectives set for this study, focused on both structural and thermal rehabilitation of the built patrimony: capacity of load transfer between layers of the sandwich panel without inclusion of metallic elements to avoid thermal bridges. The F-GFRP connectors have sufficient stiffness and strength for their required functionalities in the panel.

3.3. Polystyrene

To assess the influence of the interface between the RSFRC wythes and the core layer when subjected to shear forces, different types of polystyrene panels were considered for this experimental program. The main objective was to understand the dependence of the adhesion between RSFRC and polystyrene on the type of polystyrene material and its surface finishing. In view of this, the tests included five different types of commercially available polystyrene plates: (i) expanded polystyrene (EPS-1, Fig. 6a); (ii) extruded polystyrene with smooth surface, with parallel notches cut on both sides, with spacing of 100 mm, depth of 12.5 mm and thickness of

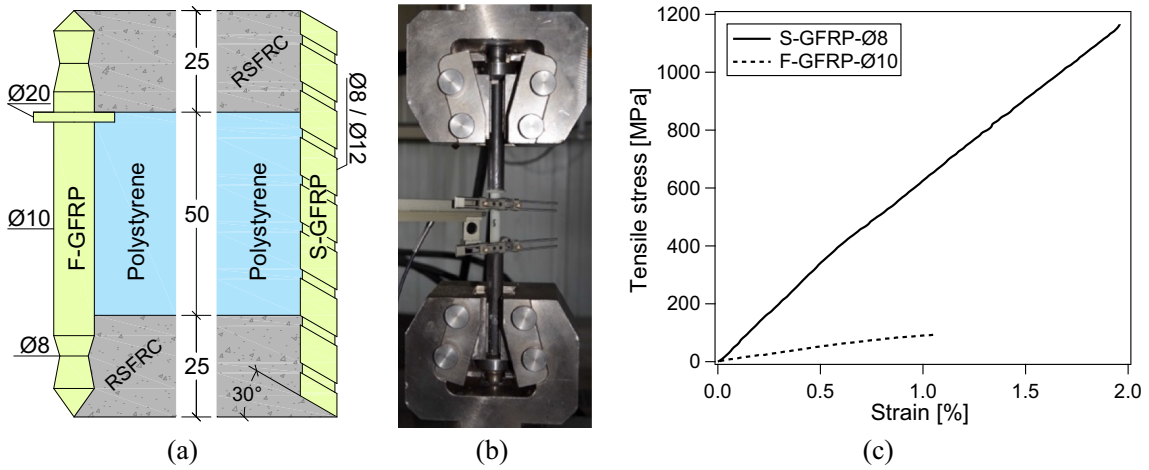

Fig. 5. Characterization of GFRP connectors: (a) Representation of F-GFRP and S-GFRP connectors on sandwich cross-section [dimensions in mm]; (b) Test setup; (c) Axial stress *vs.* strain (average curves).

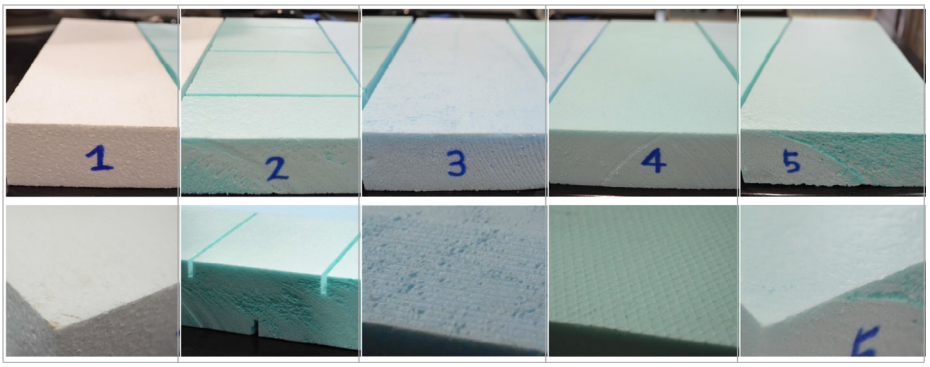

Fig. 6. Studied polystyrene typologies: (a) EPS-1; (b) XPS-2; (c) XPS-3; (d) XPS-4; (e) XPS-5.

3 mm (XPS-2, Fig. 6b); (iii) extruded polystyrene with irregular/rough surface (XPS-3, Fig. 6c); (iv) extruded polystyrene with diagonally ribbed wafer-like surface (XPS-4, Fig. 6d); and (v) extruded polystyrene with smooth surface (XPS-5, Fig. 6e). The material properties of the aforementioned polystyrene typologies, according to data provided by the suppliers [47–49], are detailed in Table 2.

4. Pushout and pullout tests on sandwich panel assemblies

4.1. Overview

This Section describes the experimental program conducted to evaluate the structural behaviour of sandwich panel assemblies, when subjected to shear loading. The experiments comprised pushout and pullout tests, which were divided in two stages: (i) pushout tests for the selection of the insulation layer of the sandwich panel under development (Section 4.2), where different types of insulation layers were assessed; and (ii) pushout and pullout tests to assist the selection of structural GFRP connectors (Sections 4.3 and 4.4, respectively), where S-GFRP connectors with different diameters (8 and 12 mm) and embedment depths (25 and 35 mm) were evaluated. The experimental program included a total of 37 specimens divided in 14 series, whose specifications are summarized in Table 3.

4.2. Pushout tests for selection of core material

4.2.1. Experimental setup and procedure

For the pushout tests, 300×300 mm^2 specimens representative of the investigated sandwich panel configuration were adopted. The geometry of the specimens is presented in Fig. 7. It can be seen that the polystyrene layer does not cover the whole extent of the specimen plan area: it is placed only in a 150 mm wide central portion of the specimen. This is due to the need for free space in the peripheral areas of the specimen, in order to ensure proper support/anchoring of the bottom RSFRC layer to the test fixture. The test setup is shown in Figs. 8a (front view) and 8b (top view), where the aforementioned anchoring system is illustrated: the bottom RSFRC layer was firmly fixed to a metallic frame with four steel plates (one near each corner), whereas the upper RSFRC layer was fixed to an actuator with 50 kN capacity, which was used to impose shear loading to the specimen (load was measured through a load cell with 25 kN capacity in tension).The tests were performed under displacement control at a rate of 5 μm/s (assessed by an LVDT with ± 0.25 μm precision, which measured the relative displacement between RSFRC wythes), as adopted elsewhere for this type of tests [50–52].

In order to study the influence of the insulation layer on the composite behaviour of sandwich panel specimens, pushout tests were performed on a total of thirteen specimens containing different types of polystyrene insulation layers, with two specimens being considered for the tests with EPS-1 and XPS-2, and three specimens being tested for each one of the remaining XPS typologies that were mentioned in Section 3.3. In order to understand the local mechanisms that govern the interaction between RSFRC, polystyrene and F-GFRP connector, the pushout tests were performed using only one connector to study its individual contribution (as an alternative to using a test setup with more connectors, potentially more stable, but of more complexity to precisely interpret their individual contribution). Hence, for all specimens, an F-GFRP connector with 10 mm of diameter was placed vertically in the geometric centre of the specimen (see Figs. 7 and 8a), bridging its constituent layers (*cf.* first part of Table 3 for additional information). An additional test was performed on a specimen without polystyrene layer (only RSFRC layers and S-GFRP connector). Due to the limited specimens available and the inherent instability of this specimen geometry (mitigated through the use of two small pieces of polystyrene, with no adherence to RSFRC), the results concerning this additional test are presented merely for the sake of comparison, as less information was retrieved, and to assist on the numerical simulations regarding the behaviour of the connector up to its failure.

Table 2
Material properties of the tested polystyrene typologies [47–49].

Material	Density [kg/m^3]	Compressive strength (10% deformation) [kPa]	Thermal conduct. [W/mK]
EPS-1	20	100	0.036
XPS-2	[30 – 33]	[200 – 300]	0.035
XPS-3	32	> 200	0.036
XPS-4	[30 – 33]	[200 – 300]	0.035
XPS-5	[30 – 33]	[200 – 300]	0.035

4.2.2. Results and failure modes

Figs. 9a, 9b, 9c, 9d and 9e present the load *vs.* horizontal relative displacement curves obtained for specimens with polystyrene typologies EPS-1, XPS-2, XPS-3, XPS-4 and XPS-5, respectively. The relative displacement is the result of the transversal deformation of the F-GFRP connector and polystyrene layer, and interfacial slip (debonding) between polystyrene and RSFRC layers. The comparison between all the tests series is shown in Fig. 9f, which depicts the average curves for each type of investigated sandwich panel configuration, including the result obtained from the specimen that did not contain a polystyrene core layer (FCØ10-H25).

Table 3
Specifications of the specimens subjected to pushout and pullout tests.

Stage of experiments	Specimen designation	N° of samples	GFRP connector	Diameter [mm]	Embedment depth [mm]	Polystyrene
Selection of insulation layer (pushout)	FCØ10-H25	1	F-GFRP	10	25	–
	FCØ10-H25-EPS1	2	F-GFRP	10	25	EPS-1
	FCØ10-H25-XPS2	2	F-GFRP	10	25	XPS-2
	FCØ10-H25-XPS3	3	F-GFRP	10	25	XPS-3
	FCØ10-H25-XPS4	3	F-GFRP	10	25	XPS-4
	FCØ10-H25-XPS5	3	F-GFRP	10	25	XPS-5
Selection of S-GFRP (pushout)	SCØ8-H25-XPS3	2	S-GFRP	8	25	XPS-3
	SCØ8-H35-XPS3	3	S-GFRP	8	35	XPS-3
	SCØ12-H25-XPS3	3	S-GFRP	12	25	XPS-3
	SCØ12-H35-XPS3	3	S-GFRP	12	35	XPS-3
Selection of S-GFRP (pullout)	SCØ8-H25	3	S-GFRP	8	25	–
	SCØ8-H35	3	S-GFRP	8	35	–
	SCØ12-H25	3	S-GFRP	12	25	–
	SCØ12-H35	3	S-GFRP	12	35	–

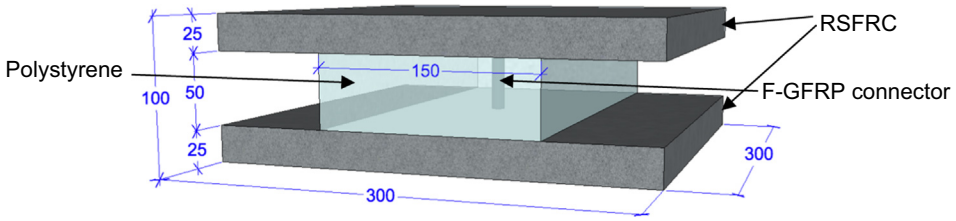

Fig. 7. Specimen geometry adopted for pushout tests [dimensions in mm].

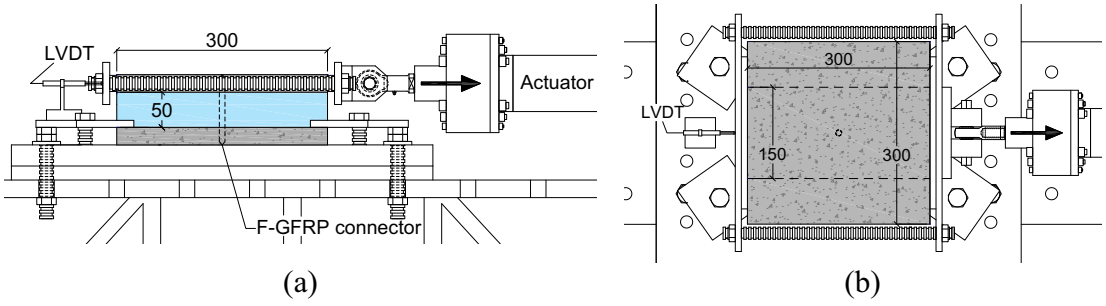

Fig. 8. Experimental setup for pushout tests with F-GFRP connectors [dimensions in mm]: (a) Front view; (b) Top view.

Fig. 10 presents a collection of photos taken before and after testing all specimen typologies, complementing the data presented in Fig. 9. Relevant results obtained for each test series, such as elastic stiffness ($k_{elastic}$), maximum load (F_{max}), relative displacement at peak load (δ_{Fmax}) and maximum relative displacement (δ_{max}), are also presented in Table 4. The maximum relative displacement, in this case, corresponds to the relative displacement for which full debonding between polystyrene and RSFRC is reached. It can be seen that specimens with core layer of type XPS-3 ensured the highest load carrying capacity until approximately 3 mm of lateral deformation, with an average peak load of 3.9 kN. The lowest structural performance was, as expected, provided by the specimen that did not contain a polystyrene layer (only 0.8 kN of maximum load), followed by specimens with insulation type XPS-5 (XPS with smooth surface finishing, for which a peak load of 1.3 kN was attained).

In general, the structural behaviour of the various sandwich panel assemblies when subjected to shear loading can be described by the following four main phases (identified for specimens XPS-4, as an example - see Fig. 9d): (i) linear behaviour until approximately [0.5–1.5] mm of relative displacement between wythes; (ii) beginning of non-linearity triggered by stiffness reduction, then followed by a load decrease after initiation of the debonding process between the bottom RSFRC and its contacting polystyrene (the load decrease is steeper for polystyrene typologies that provide better adhesion to the RSFRC wythes, since this also ensured higher peak load); (iii) hardening phase in the post-peak stage, characterized by a gradual load increase due to friction at the RSFRC-polystyrene interfaces that takes place during the continuing debonding process; and (iv) softening phase, initiated after failure of the F-GFRP connector at the bottom RSFRC-polystyrene interface (see Figs. 10c, 10f, 10i, 10l and 10o) that occurs between approximately 10 and 12 mm of relative displacement, until full debonding of the bottom RSFRC-polystyrene interface (see Figs. 10b, 10e, 10h, 10k and 10n).

When analysing the differences obtained for the different specimen typologies, it can be seen that, for specimens with EPS only partial debonding occurred (in approximately half of the RSFRC-polystyrene interface area), with actual shear failure taking place in the polystyrene layer itself, near the interface, as illustrated in Fig. 10b (a small portion of EPS remained attached to the bottom RSFRC layer). Through the analysis of all tested specimens it was verified that XPS-5 specimens presented the "cleanest" bottom polystyrene surface (perfect separation between RSFRC and

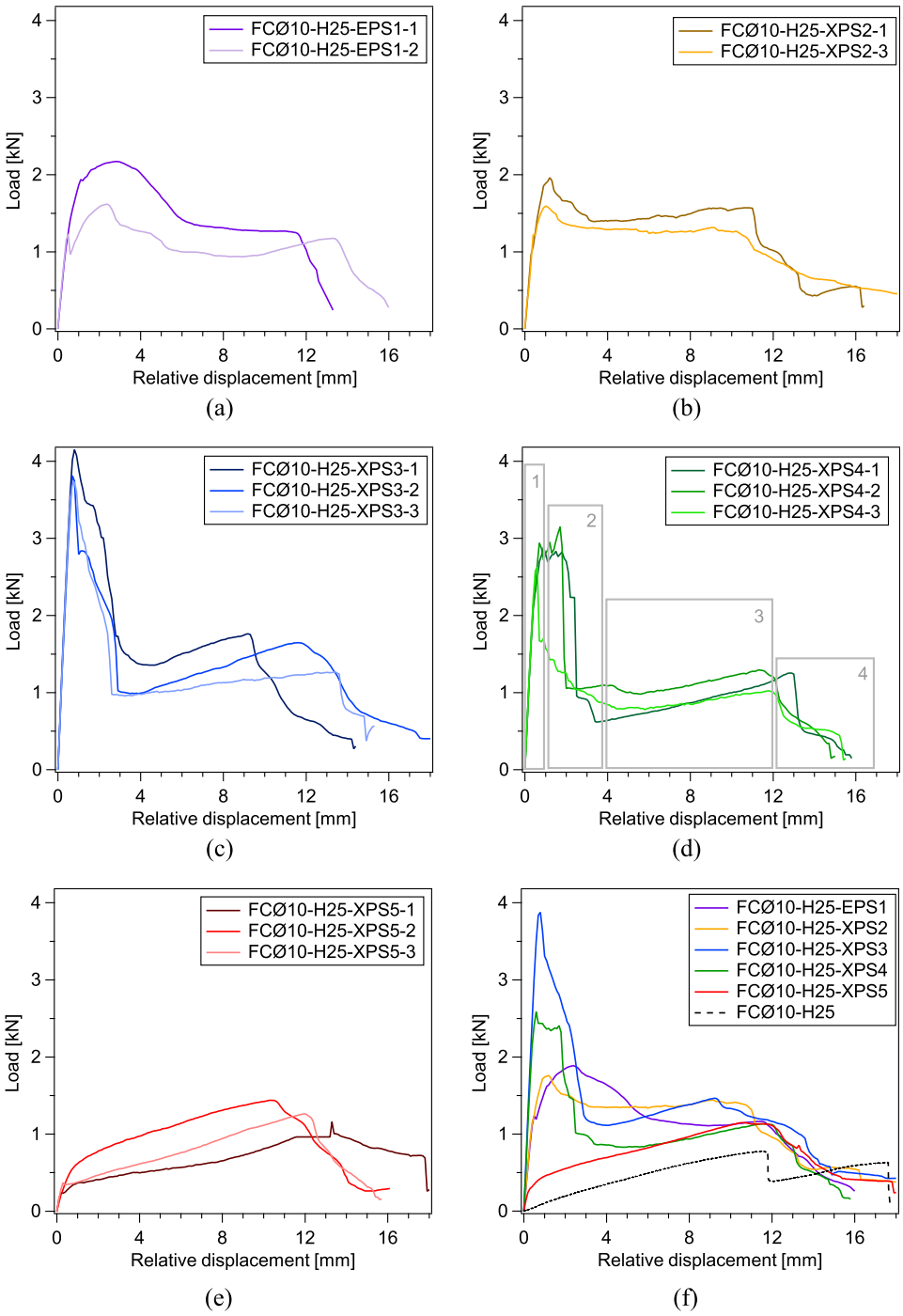

Fig. 9. Pushout tests on specimens with different polystyrene typologies – load *vs.* relative displacement responses for: (a) EPS-1; (b) XPS-2; (c) XPS-3; (d) XPS-4; (e) XPS-5; (f) average curves.

XPS – see Fig. 10n), which indicates that this polystyrene typology provided the smallest adhesion to the RSFRC. In fact, particular disparities were observed in case of XPS-5 when compared to the remaining typologies, for which the linear/non-linear transition loading state was reached at a significantly lower load (approximately 0.3 kN) and was followed by a hardening response (the load has increased with the relative displacement) in the above-mentioned second phase, rather than a softening response, observed in the tests of the other polystyrene systems. Also, for XPS-5, the maximum load was reached at the point of F-GFRP connector failure (already described in this section), corresponding to approximately 12 mm of relative displacement. This behaviour has similarities with the specimen that was tested without polystyrene layer (see Fig. 9f and Table 4). It is worth highlighting that among the two most commonly used polystyrene solutions, namely specimens EPS-1 and XPS-5, EPS provided significantly higher shear strength to the composite solution (+50%), which may be justified by the higher adhesion between EPS (*vs.* XPS with smooth surface finishing) and RSFRC. Overall, based on the obtained results (best results until the end of phase 2 were obtained for XPS-3, XPS-4 and EPS-1), irregular surface finishing proved to be a relevant parameter to be taken into consideration for the selection of the

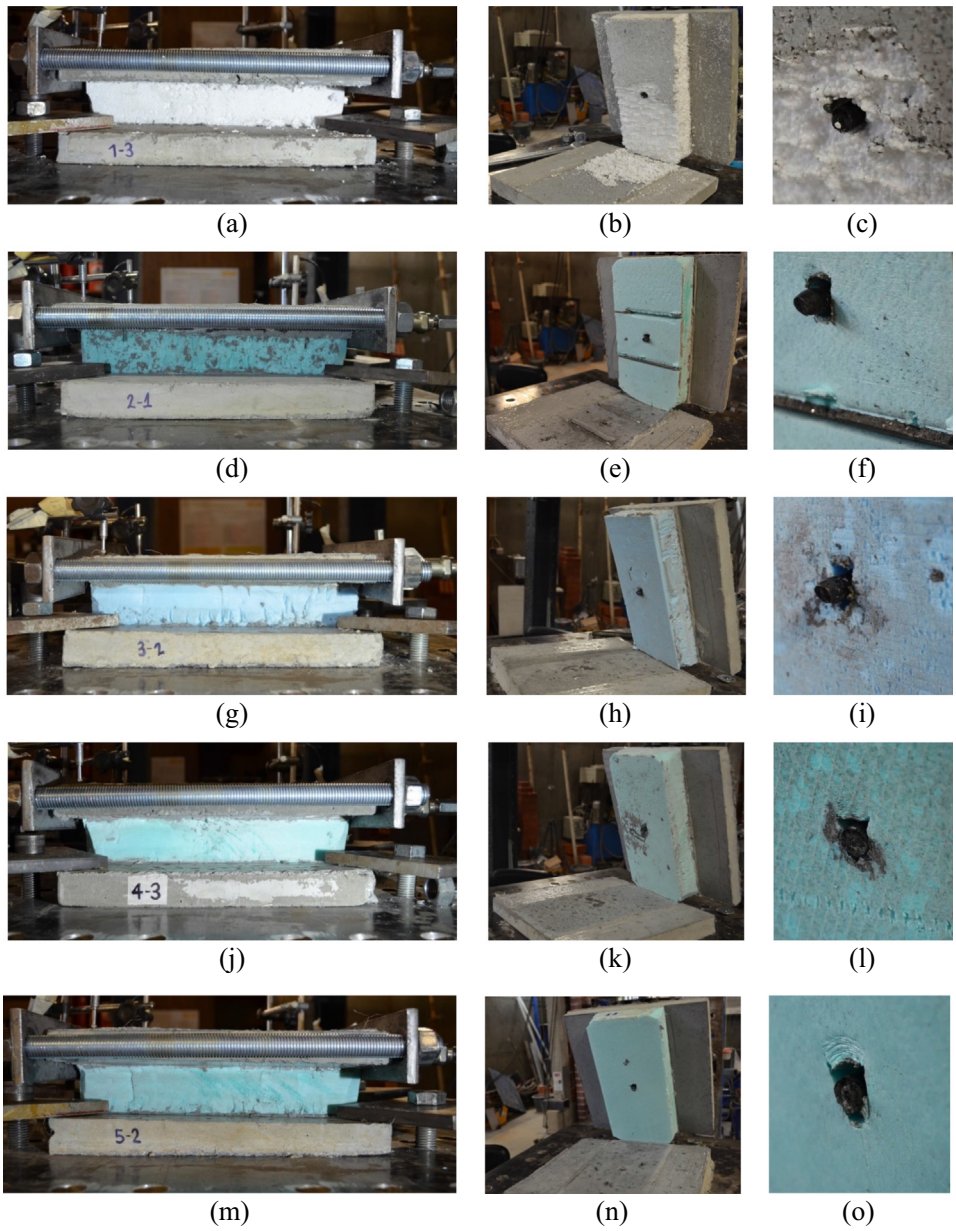

Fig. 10. Pushout tests for selection of insulation layer. Specimens before (left) and after testing (centre and right): (a, b, c) EPS-1; (d, e, f) XPS-2; (g, h, i) XPS-3; (j, k, l) XPS-4; (m, n, o) XPS-5.

Table 4
Pushout tests: Relevant results obtained for all specimen typologies (average values).

Specimen designation	$k_{elastic}$ [kN/m]	F_{max} [kN]	$\delta_{F,max}$ [mm]	δ_{max} [mm]
FCØ10-H25	99	0.8	11.7	17.7
FCØ10-H25-EPS1	2768	1.9	2.6	14.4
FCØ10-H25-XPS2	3413	1.8	1.3	15.6
FCØ10-H25-XPS3	6305	3.9	0.8	16.0
FCØ10-H25-XPS4	5623	2.9	1.1	15.4
FCØ10-H25-XPS5	1437	1.3	11.9	16.6
SCØ8-H25-XPS3	7265	6.7	14.8	37.2
SCØ8-H35-XPS3	8767	8.4	18.2	19.2
SCØ12-H25-XPS3	8870	7.7	3.4	37.9
SCØ12-H35-XPS3	13205	9.9	6.2	33.7

polystyrene typology. Further investigations comprising the detailed characterization of surface roughness should focus on optimizing the surface pattern of polystyrene plates. Parametric studies with the model described in Section 5 will allow to optimize the bond conditions between core materials and RSFRC layers in terms of target performing indexes.

4.3. Pushout tests for selection of structural GFRP connectors

4.3.1. Experimental setup and procedure

The overall geometry of the specimens (see Fig. 7) and experimental setup adopted for the second stage of pushout tests were equivalent to those used in the first one (*cf.* Section 4.2.1), with just a slight difference regarding the test setup: the anchoring of the bottom RSFRC layer was achieved using two 560 mm long steel plates (which cover the two longitudinal borders of the specimens – see Fig. 11), rather than one steel plate at each corner. The tests were also conducted under displacement control, at a rate of 5 μm/s, up to 20 mm; thereafter, the speed was increased to 10 μm/s until specimen failure.

Compared to the first series of tests, the second series of pushout tests were performed with focus on the enhancement of structural performance provided by the use of S-GFRP connectors. Hence, and as shown in the second part of Table 3, the same type of polystyrene typology was adopted for all specimens, namely XPS-3 (the one that provided the highest load carrying capacity – see Fig. 9f), while varying the diameter (8 mm and 12 mm) and embedment depth (25 mm and 35 mm) of the S-GFRP connectors. The four specimen typologies considered for this study are depicted in Fig. 12, which provides, for each specimen typology, a 2D representation of Section A-A' (indicated in Fig. 11b) and a 3D illustration (front view of the specimen). Note that to assure an embedment length of 35 mm to the connectors, the RSFRC layers are locally thicker in the vicinity of the connector (visible in Figs. 12b and 12d). This geometrical detail can potentially increase the local frictional resistance provided by the XPS layer.

The shear interaction performance of sandwich panels using structural GFRP connectors with different geometric configurations and arrangements has been widely studied in the literature by performing pushout tests [29–31,34,36,53]. However, the majority of studies report concrete wythes of plain concrete reinforced with steel rebars or meshes. To the author's best knowledge, no studies have been performed where the sandwich panel concept involves GFRP connectors in combination with thin concrete wythes reinforced with recycled steel fibres.

4.3.2. Results and failure modes

Figs. 13a, 13b, 13c and 13d present the load *vs.* horizontal relative displacement curves for series SC-Ø8-H25-XPS3, SC-Ø8-H35-XPS3, SC-Ø12-H25-XPS3 and SC-Ø12-H35-XPS3, respectively. The comparison between all test series is shown in Fig. 13e, where the average curves obtained from all pushout tests (including pushout test with XPS-3 reported in Section 4.2) are presented. The summary of results obtained for each test series is also included in Table 4, where, for this series of pushout tests, maximum relative displacement (δ_{max}), corresponds to the relative deformation for which specimen failure occurs or, in case of gradual load decline, when applied load becomes lower than 1 kN. Photos of a representative test specimen before and during the experimental procedure are shown in Figs. 14a and 14b, respectively. Since only one connector was used, placed at the centre of the specimens, a slight (not measured) rotation between whytes was observed (visible in Fig. 14b). However, the setup was stable enough to provide reliable results.

The structural behaviour of the various sandwich panel specimens containing S-GFRP connectors can be described by the following four main phases: (i) linear-elastic behaviour until approximately 0.65 mm of relative displacement between wythes; (ii) beginning of non-linearity with slight stiffness reduction (due to initial damage in the RSFRC matrix, near the anchorage zone) until a first peak load is reached; (iii) an almost load plateau phase up to approximately 16 mm of relative displacement between wythes in the series SC-Ø8-H25-XPS3, SC-Ø8-H35-XPS3 and SC-Ø 12-H35-XPS3 (see deformed specimen in Fig. 14b); and (iv) softening phase until specimen failure, which is reached earlier for specimens with higher embedment length. Test series SC-Ø 12-H25-XPS3 (see Fig. 13c) had a very small load plateau phase (ended at about 5 mm of relative displacement) due to the relatively high stiffness of this connector (12 mm diameter), together with the relatively small embedment length (25 mm), resulting in larger damage in the RSFRC anchorage area.

Fig. 15 shows the damage patterns for each specimen typology after testing (the polystyrene layer was removed to enable a clearer observation), with emphasis on both the RSFRC layers (left-hand side of Fig. 15) and the S-GFRP connectors (right-hand side of Fig. 15). The figure prompts the following remarks: (i) specimens of typology SC-Ø8-H25-XPS3 exhibit minor RSFRC spalling near the anchorage areas (Fig. 15a) and visible damage in the S-GFRP connectors (splitting of the connector in its longitudinal direction – Fig. 15b); (ii) shear failure of the S-GFRP connectors occurred for specimens of typology SC-Ø8-H35-XPS3 (rupture of the connector is visible in Fig. 15c and 15d), in contrast with the remaining specimen typologies for which higher ductility was obtained and failure was due to gradual debonding of the upper GFRP-RSFRC connection; (iii) specimens of typology SC-Ø12-H25-XPS3 present visible cracks and spalling of the RSFRC layer (see Fig. 15e) and the lowest damage level on the S-GFRP connectors (see Fig. 15f), which explains the more pronounced softening phase for this specimen configuration (the shear capacity of the S-GFRP connector was not mobilized, being the spalling and crushing of the RSFRC the weakest characteristics of this connection system); and (iv) SC-Ø12-H35-XPS3 specimens afforded the highest load carrying capacity up to approximately 24 mm of relative displacement between RSFRC wythes, reaching an average peak load of 9.9 kN and presenting damage both in the RSFRC layer (see in Fig. 15g the radial cracks that formed in the augmented anchorage depth zone) and in the S-GFRP connector (splitting of the connector due to formation of multiple longitudinal cracks during the plateau phase – Fig. 15h). This last connection system provided the

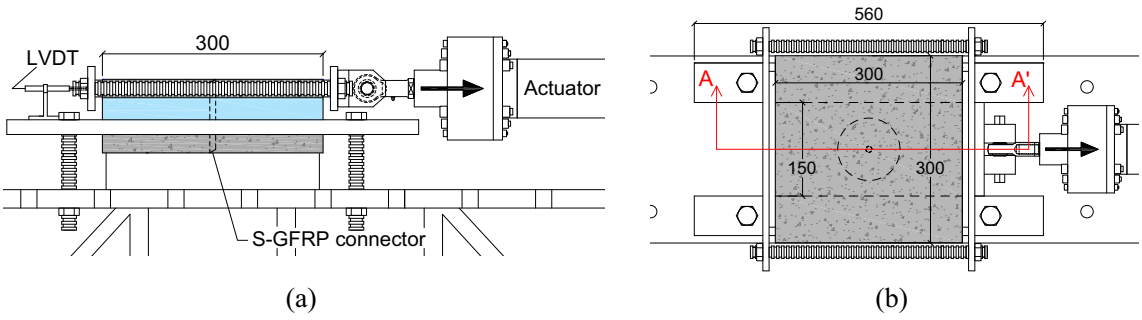

Fig. 11. Experimental setup for pushout tests with different S-GFRP connectors [dimensions in mm]: (a) Front view; (b) Top view.

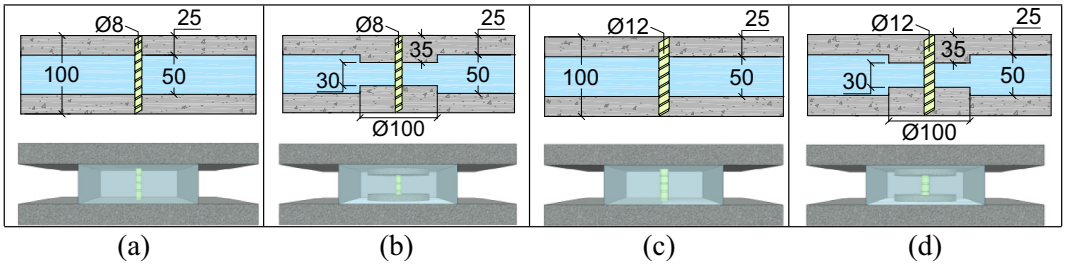

Fig. 12. Specimen typologies for pushout tests with different S-GFRP connectors [dimensions in mm]: (a) SC-Ø8-H25-XPS3; (b) SCØ8-H35-XPS3; (c) SCØ12-H25-XPS3; (d) SCØ12-H35-XPS3.

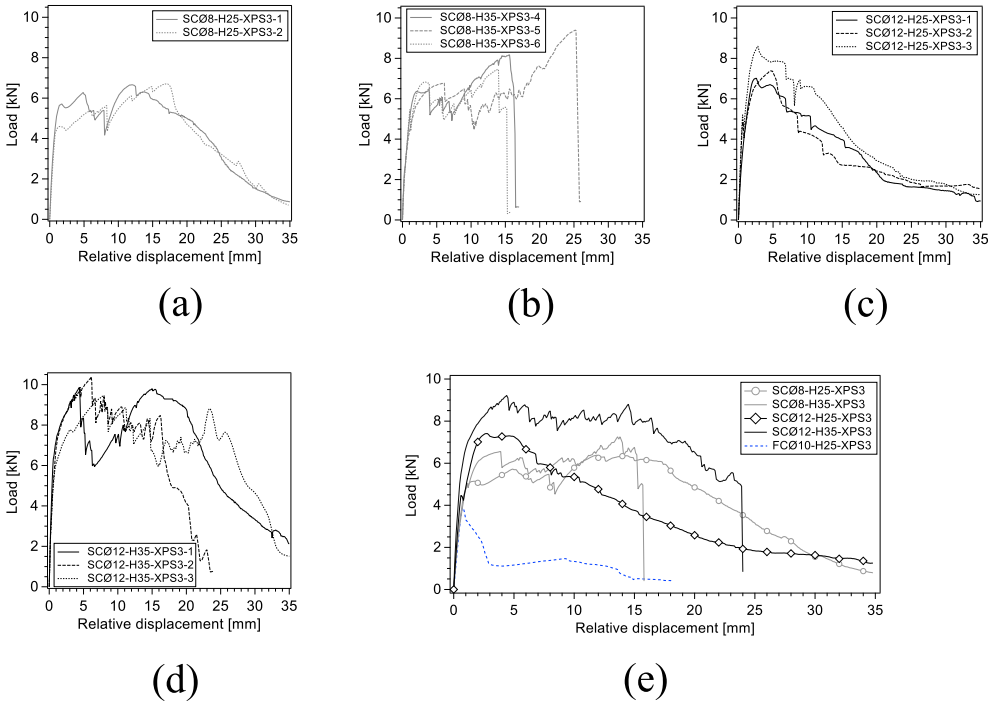

Fig. 13. Pushout tests on specimens with different S-GFRP connectors – load *vs.* relative displacement responses for: (a) SC-Ø8-H25-XPS3; (b) SC-Ø8-H35-XPS3; (c) SC-Ø12-H25-XPS3; (d) SC-Ø12-H35-XPS3; (e) average curves.

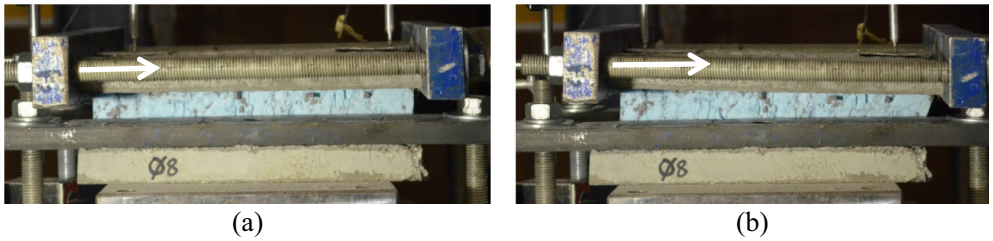

Fig. 14. Pushout tests on specimens with different S-GFRP connectors: specimen before (a) and during (b) testing procedure (for an imposed displacement equal to 16 mm).

highest shear load transfer, pseudo-ductility and energy absorption, due to the full exhaustion of the S-GFRP connector and the surrounding RSFRC, being therefore the most appropriate arrangement for structural purposes. However, it should be noted that materializing the thicker part of the RSFRC for ensuring a thickness of 35 mm has detrimental consequences on execution time and costs of the type of panel in development. In view of this, SC-Ø8-H25-XPS3 is regarded as a more rationally balanced system, as long as the shear load per connector does not exceed 5 kN.

4.4. Pullout tests for selection of structural GFRP connectors

4.4.1. Experimental setup and procedure

In order to obtain comprehensive information to make a well-supported decision on the type of S-GFRP connectors for the sandwich panel in development, pullout tests were conducted to assess the bond performance of this type of connectors to RSFRC. Figs. 16a and 16b illustrate the setup of these tests. The parameters considered in the pushout test program, namely the diameter and embedment depth (see Table 3), were also adopted in the pullout

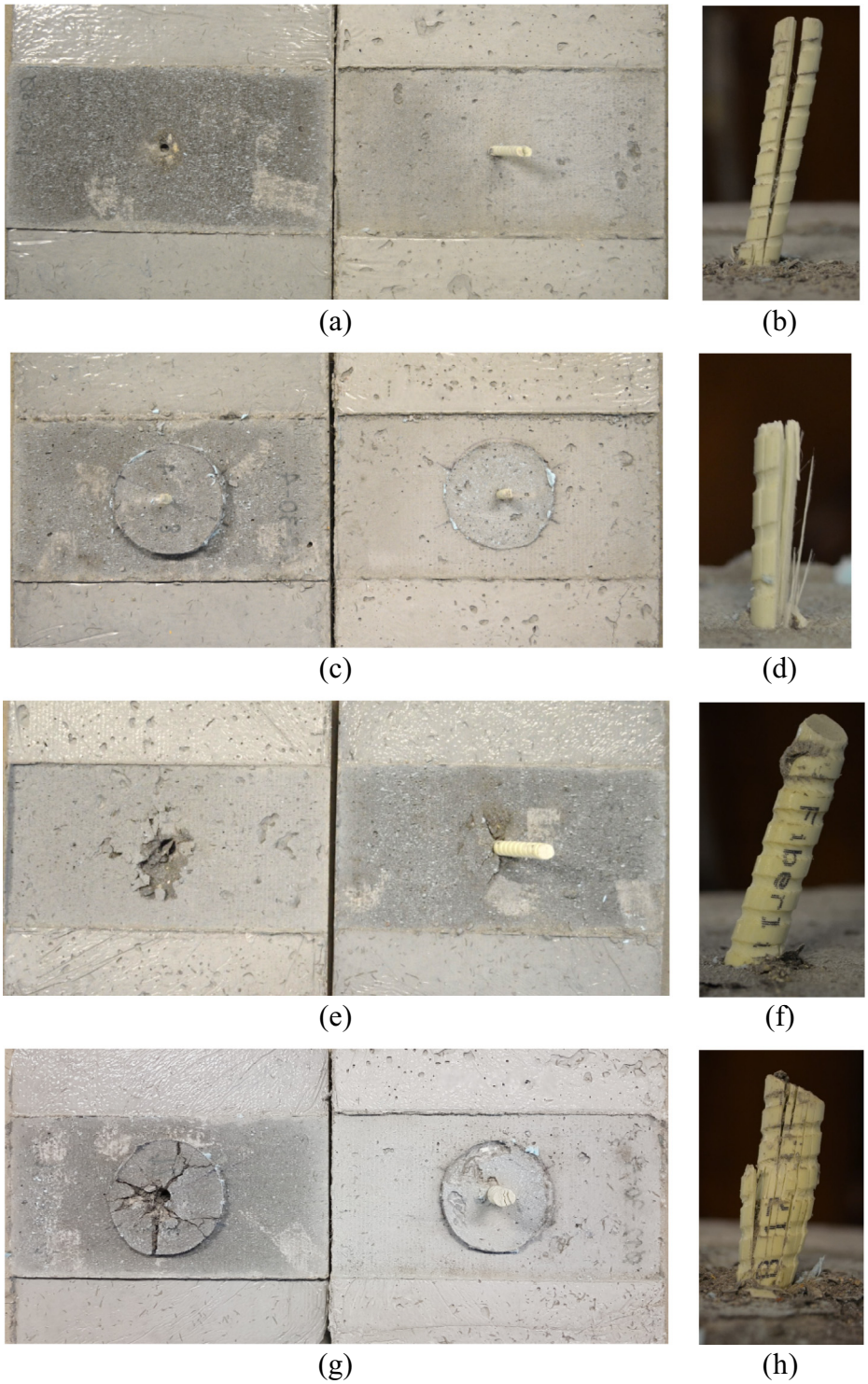

Fig. 15. Pushout tests using different S-GFRP connectors (photos showing damage state of tested specimens): (a, b) SC-Ø8-H25-XPS3; (c, d) SC-Ø8-H35-XPS3; (e, f) SC-Ø12-H25-XPS3; (g, h) SC-Ø12-H35-XPS3.

test program, with 3 specimens for each parameter value, resulting in a total of 12 tests. It should be noted that, due to the reduced length of the GFRP connectors (100 mm), the end part of the connectors had to be surrounded by a Steel Hollow Section (SHS) profile, bonded to the GFRP connector with epoxy adhesive [54] (see Fig. 16c). This was done to provide higher contact area between the grip of the testing equipment and the GFRP connector (the grip is clamped around the SHS profile, as shown in Fig. 16a). Due to space restrictions, it was impossible to use additional LVDTs for measuring exclusively the slip between the S-GFRP and the surrounding RSFRC during the pullout test. Therefore, presented results only include information regarding load application (measured by a load cell of 50 kN capacity) and additional measurements conducted after performing the pullout tests. The pullout tests were performed under displacement control, at a rate of 10 μm/s.

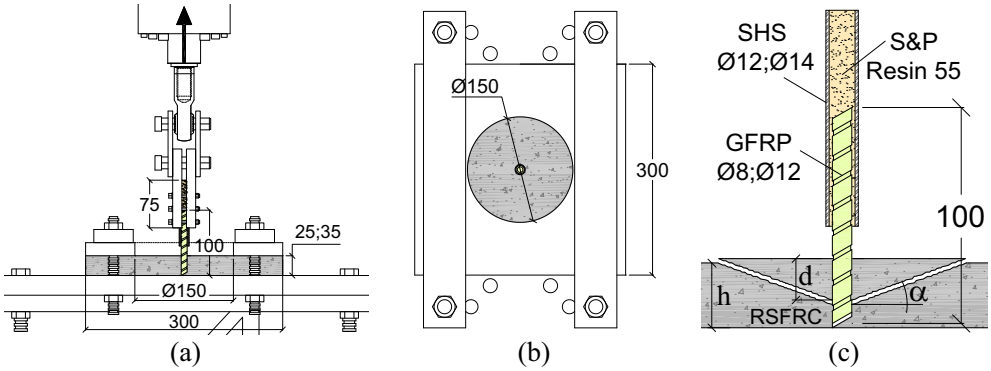

Fig. 16. Experimental setup for pullout tests with different S-GFRP connectors [dimensions in mm]: (a) Front view; (b) Top view; (c) Detailed view of GFRP connector.

4.4.2. Results and failure modes

Fig. 17 presents the maximum pullout force that was obtained during the pullout tests for all specimens. Average values for each specimen typology are presented in Table 5. All specimens failed by debonding between the S-GFRP connector and the surrounding RSFRC, followed by the formation of a *quasi*-concrete cone that disintegrated by microspalling (see Fig. 18). Additional information concerning the registered failure mode is also provided in Table 5 (equivalent concrete cone diameter, cone depth and cone angle, as depicted in Fig. 16c). The equivalent concrete cone diameter was determined by the average value resultant from four measurements that were taken on each of the tested specimens, as shown in Fig. 18d.

Minimum pullout force was expectably obtained for test series SC-Ø8-H25, registering an average load equal to 9.3 kN. For the remaining test series SC-Ø8-H35, SC-Ø12-H25 and SC-Ø12-H35, average pullout forces equal to respectively 10.3, 11.2 and 13.1 kN were registered. It can also be seen that the increase of embedment depth (RSFRC thickness) had a more pronounced effect for the case of connectors with 12 mm of diameter, resulting in an increase of pullout force of approximately 17% (only 10% in the case of SCØ8). Assuming that at peak load no spalling has occurred in the RSFRC, and considering the embedment depth for the S-GFRP registered in the post-inspection tests, an average bond strength varying between 10.2 and 13.5 MPa was obtained, with a decreasing trend with the increase of the S-GFRP diameter and embedment depth. It would have been possible to derive a local bond constitutive law by an inverse analysis technique, such as the one described in [55]; however, loaded end slip would have to be measured together with the applied force – future experiments should be conducted in this respect.

4.5. Summary and design of the connectors

In view of the results that were obtained from the pushout and pullout tests, preliminary numerical simulations (not reported in detail due to paper length limitations) have been conducted in order to determine the number of structural GFRP connectors that need to be incorporated in the sandwich panel. Assuming linear elastic behaviour for all the constituent materials of the panel and partial safety factors of 1.5 for load effects and resistances, the number of connectors was evaluated for the following three scenarios: (i) manufacturing and transportation process (lifting operations after completion of casting process); (ii) on site installation process (handling of the sandwich panel during retrofitting process of existing building envelope); and (iii) wind action (out of plane pressure loads). Obtained results show that approximately 2.7 connectors per square meter of sandwich panel are required to withstand shear and tensile loads in the RSFRC-GFRP connection induced by the referred design scenarios. Hence, the use of at least 12 uniformly distributed S-GFRP connectors, with minimum distances of 300 mm between connectors and 150 mm between connectors and sandwich panel edges, allows fulfilling safety verifications while ensuring an adequate load distribution in the RSFRC layers.

5. Numerical simulations

5.1. Introduction

For assessing the relevant properties of the bond conditions between RSFRC layers and the core material, material nonlinear

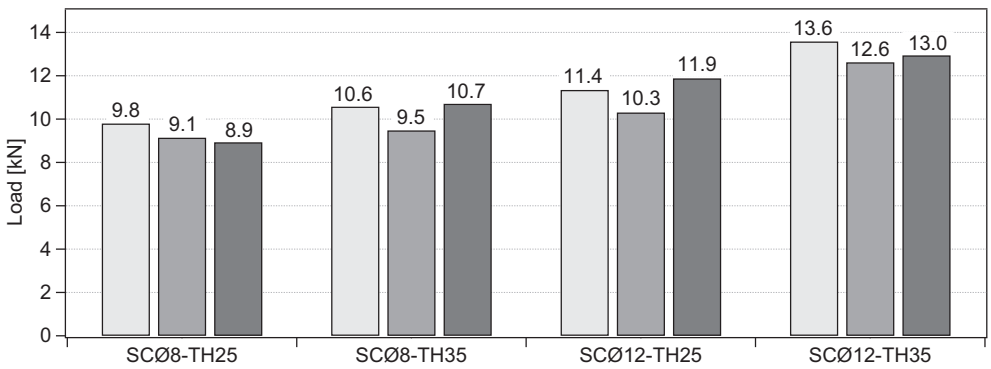

Fig. 17. Maximum pullout force obtained during pullout tests (for all specimens).

Table 5
Pullout tests: relevant results for tested specimen typologies (average values).

Specimen designation	F_{max} [kN]	Embedment depth (h) [mm]	Average bond strength [MPa]	Cone diameter [mm]	Cone depth (d) [mm]	Cone angle (α) [°]
SCØ8-H25	9.3	27.4	13.5	62.0	18.5	17.1
SCØ8-H35	10.3	34.4	11.9	62.2	20.4	18.8
SCØ12-H25	11.2	26.9	11.0	81.1	22.2	15.6
SCØ12-H35	13.1	34.2	10.2	90.0	25.7	16.1

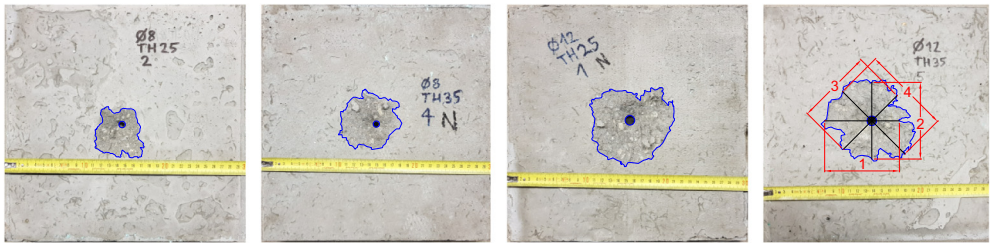

Fig. 18. Pullout tests using different S-GFRP connectors (photos showing damage state on RSFRC layer): (a) Ø8-H25; (b) Ø8-H35; (c) Ø12-H25; (d) Ø12-H35.

finite element analyses with the FEMIX computer program [56] were carried out. The derived information can be of paramount relevance in future numerical simulations for assessing the strengthening effectiveness of the sandwich panel that is been developed under the framework of seismic retrofitting of the target buildings referred in Section 1. Taking into account that the pushout tests that were performed for selection of the core material, the numerical simulation reported herein attempts to capture the experimental behaviour obtained for specimen typology FCØ10-H25-XPS3 (best performance in terms of bond between RSFRC and polystyrene). As mentioned in Section 4.2.2, the failure mechanisms of this specimen were governed by a coupled effect of sliding-opening at the interface between the bottom layer of the RSFRC and XPS-3, together with the rupture of the connector at relatively large sliding of the top RSFRC layer. Therefore, for modelling these complex failure mechanisms, a constitutive model for a 3D interface finite element (IFE) was selected, capable of coupling the opening-sliding effects by considering the tensile strength, cohesion and internal friction angle, as well as their evolution properties during the opening-sliding process.

5.2. Constitutive model for surface interface finite element

In this section a brief overview of the main features of the adopted constitutive model is provided. Further details can be consulted elsewhere [57,58]. The constitutive model is prepared for simulating the contact between bodies discretized by solid finite elements, therefore three stress components ($\underline{\sigma} = [\,\sigma_n \quad \tau_{t_1} \quad \tau_{t_2}\,]^T$) and corresponding displacements ($\underline{u} = [\,u_n \quad u_{t_1} \quad u_{t_2}\,]^T$) can be installed in the corresponding IFE (see Fig. 19).
Before the criterion of movement separation of the faces of this IFE has been violated, this "zero-thickness" IFE is modelled by the following linear-elastic stiffness matrix:

$$K_{el} = \begin{bmatrix} k_n & 0 & 0 \\ 0 & k_{t_1} & 0 \\ 0 & 0 & k_{t_2} \end{bmatrix} \tag{1}$$

where k_n, k_{t_1} and k_{t_2} represent the elastic stiffness in the orthogonal, and in the t_1 and t_2 tangential directions, respectively. Adequate values for these elastic stiffness components should be provided for avoiding interpenetration of the bodies in contact (too low values) or numerical instabilities (too high values).

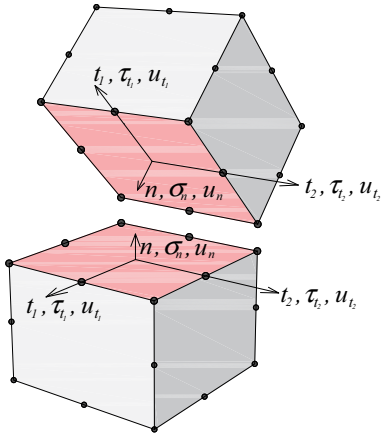

Fig. 19. Stress and displacement components in the surface interface finite element.

For modelling the movement of the two faces in contact of the IFE, the following hyperbolic cracking failure surface is adopted [57]:

$$F(\underline{\sigma}, \underline{r}_F) = \sqrt{(\tau_{t_1})^2 + (\tau_{t_2})^2 + (c_F - f_{t,F}tan\phi_F)^2} - (c_F - \sigma_n \tan\phi_F) \tag{2}$$

where $f_{t,F}$ is the tensile strength, c_F is the asymptotic cohesion, and $\tan\phi_F$ is the asymptotic friction angle, being collected in the vector $\underline{r}_F = [f_{t,F}, c_F, \tan\phi_F\,]^T$.

For modelling the dilatancy effect due to the roughness of the faces in contact, which leads to the separation of these faces (opening) with the sliding, a process that is also influenced by the applied orthogonal stress, σ_n, a non-associated formulation is adopted by considering the following plastic potential function:

$$P(\underline{\sigma}, \underline{r}_P) = \sqrt{(\tau_{t_1})^2 + (\tau_{t_2})^2 + (c_P - f_{t,P}tan\phi_P)^2} - (c_P - \sigma_n \tan\phi_P) \tag{3}$$

that is formally equal to the cracking failure surface (Eq. (2)), but now defined from the parameters $\underline{r}_P = [f_{t,P}, c_P, \tan\phi_P\,]^T$. In the present formulation it is assumed that $f_{t,F} = f_{t,P} = f_t$.

The evolution of the cracking surface, F=0, and plastic potential, Q=0, is governed by the hardening parameters, $\underline{r}_\alpha = [f_t, c_\alpha, \tan\phi_\alpha]^T$ with α=F or P, according to the following equations:

$$\xi_I = \begin{cases} \frac{1}{2} - \frac{1}{2}\cos\left(\frac{\pi W^{cr}}{G_{F,I}}\right) & 0 \leqslant W^{cr} \leqslant G_{F,I} \\ 1 & W^{cr} > G_{F,I} \end{cases} \quad (4)$$

and

$$\xi_{II} = \begin{cases} \frac{1}{2} - \frac{1}{2}\cos\left(\frac{\pi W^{cr}}{G_{F,II}}\right) & 0 \leqslant W^{cr} \leqslant G_{F,II} \\ 1 & W^{cr} > G_{F,II} \end{cases} \quad (5)$$

where $G_{F,I}$ and $G_{F,II}$ are the fracture energy in mode I and mode II, respectively, being assumed that $G_{F,II}$ is the same in the t_1 and t_2 tangential directions to the plane of the interface. In Eqs. (4) and (5), W^{cr} is the work produced during the fracture process, being the unique internal history variable controlling the evolution of cracking surface and potential plastic functions, determined from:

$$dW^{cr} = \begin{cases} \sigma_n du_n^{cr} & \sigma_n \geqslant 0 \quad \text{(tension)} \\ (\| \tau \| + \sigma_n \tan\phi) \| du_t^{cr} \| & \sigma_n < 0 \quad \text{(compression)} \end{cases} \quad (6)$$

where

$$\| \tau \| = \sqrt{(\tau_{t_1})^2 + (\tau_{t_2})^2} \quad (7a)$$

$$\| du_t^{cr} \| = \sqrt{\left(u_{t_1}^{cr}\right)^2 + \left(u_{t_2}^{cr}\right)^2} \quad (7b)$$

being $\underline{u}^{cr} = \underline{u} - \underline{u}_{el}$ the post-cracking displacement components.

The evolution of the materials parameters with the work produced during the fracture process is simulated by the same type of function (except for the friction angle of the plastic potential):

$$\chi = \chi_0[1 - f(\xi_i)] \quad (8)$$

where χ can represent f_t, c_α or $\tan\phi_F$, and, accordingly, χ_0 will represent the initial tensile strength ($f_{t,0}$), the initial cohesion ($c_{0,\alpha}$), and the tangent of the initial friction angle for the cracking surface ($\tan\phi_{0,F}$). When Eq. (8) is used for modelling the evolution of the tensile strength, $\xi_i = \xi_I$, while when adopted for simulating the evolution of both the cohesion and the friction angle, $\xi_i = \xi_{II}$.

Finally, the evolution of the friction angle in the plastic potential function is simulated by the following equation:

$$\tan\phi_P = \tan\phi_{0,P} - (\tan\phi_{0,P} - \tan\phi_r) f(\xi_{II}) \quad (9)$$

where $\tan\phi_{0,P}$ and $\tan\phi_r$ are the tangent of the initial and residual friction angle, respectively.

The scaling function $f(\xi_i)$ in Eq. (8) is obtained from:

$$f(\xi_i) = \frac{e^{-\lambda}\xi_i}{1 + (e^{-\lambda} - 1)\xi_i} \quad (10)$$

where λ is the softening parameter that define the damage evolution of the $\underline{r} = [f_t, c, \tan\phi]^T$ variables. The damage evolution for the tensile strength, cohesion and friction angle can be different by adopting distinct values for the corresponding λ parameter (λ_{f_t}, λ_c, $\lambda_{\tan\phi}$).

5.3. Simulations and analysis

Due to the symmetry of experimentally testing conditions, only half of the specimen was simulated, by using the finite element mesh represented in Fig. 20, where the type of finite elements, support and loading conditions are indicated. Both the core material (XPS-3) and the two outer RSFRC layers were modelled by solid serendipity finite elements of 20-nodes with 2×2×2 Gauss Legendre integration scheme (GL-IS), while surface interface serendipity finite elements of 16 nodes were adopted in the contact between the bottom RSFRC and the XPS-3 layers, by using 2×2 GL-IS. The experimental tests demonstrated that no movement occurred between the top RSFRC layer and the XPS-3, therefore perfect bond conditions were assumed for this contact zone.

Taking into account the results obtained in the pushout test with a specimen where the two outer RSFRC layers were exclusively connected by the S-GFRP connector (FCØ10-H25 in Fig. 9f), the axial and shear stiffness provided by this connector were considered in the numerical model for replacing the connector by equivalent springs, since this strategy can reproduce effectively the contribution of the connector up to its rupture, with benefits in terms of computing time (see Fig. 21). The complex behaviour of the connector was simulated by a trilinear diagram defined by the branches OP, PS and SR. The point S is located in the branch PQ and was determined in order that the areas A_1 and A_2 would be approximately equal, by pivoting in the point R, corresponding to the full rupture of the connector. This strategy aims at simulating the last complex stage of the behaviour of the connector by an equivalent softening modulus. The values of displacement and corresponding force for the points P, S and R define the trilinear load–displacement diagram for the spring simulating the shear contribution of the connector. The axial stiffness of this connector was also simulated by a spring (in X_3 direction) connected to the point (blue circle) indicated in Fig. 20, by assuming linear-elastic behaviour in tension up to its rupture (at an elongation of 0.9 mm). Displacements in the X_2 direction were imposed in the face of the top RSFRC layer in contact with the actuator (see Fig. 20).

Table 6 indicates the values adopted for the IFE model parameters. The values were estimated by considering the material properties [47] and experimental results obtained for XPS-3 and based on information published by other researchers [59–61]. For the adopted values, the evolution of the normalized model's parameters (χ/χ_0), namely cohesion and friction angle for the cracking failure surface, with $W^{cr}/G_{F,I}$ are represented in Figs. 22a and 22b, respectively. It is verified that the decrease of the cohesion with the work produced during the fracture process (W^{cr}) was less abrupt than in the case of the friction angle.

Fig. 23 compares the load *vs.* relative lateral displacement recorded experimentally and obtained numerically, where it can be seen that the adopted model with the considered parameter values is capable of reproducing the main behavioural features registered in the experimental tests. The influence of the connector is only mandatory for a deflection level above the one corresponding to point C. The three branches between the peak point and point C registered experimentally were not captured with precision due to the continuous nature of the functions of the adopted formulation.

6. Conclusions

This paper presented a concept of a multi-functional sandwich panel comprising external RSFRC layers, a polystyrene inner core insulation and GFRP connectors. This sandwich panel aims to be the main construction system of integrated rehabilitation (structural and thermal) of multi-storey RC-frame buildings characteristic from the 1960s to 1980s, deficiently designed for seismic conditions. The experiments presented in this paper focused mainly (i) on the characterization of the behaviour of the panels' individual components, and also (ii) on the shear connection behaviour of the panels, namely on the influence of the type of insulation layer and the type of GFRP connector. Based on the experimental results, the following main conclusions can be drawn:

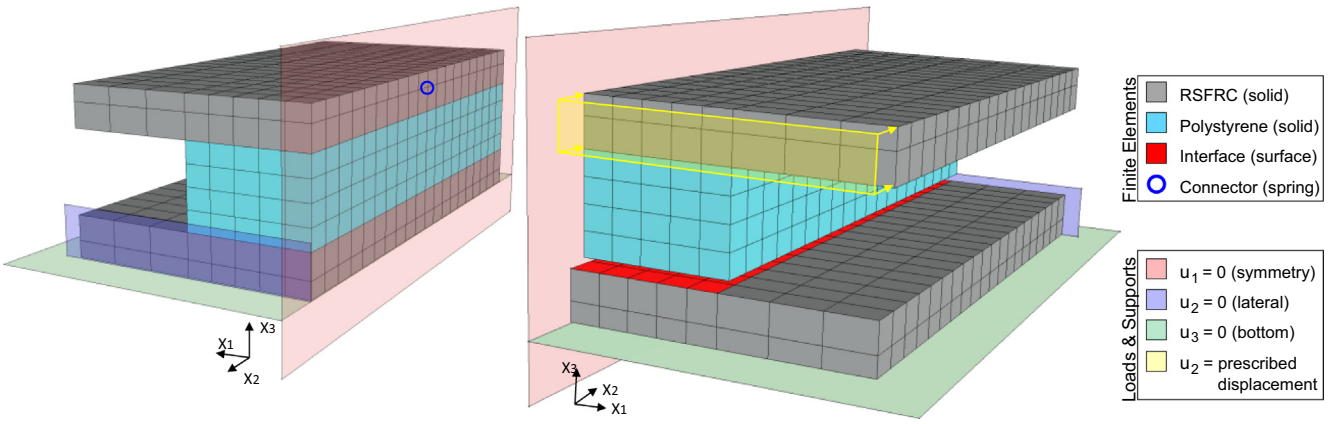

Fig. 20. Finite element mesh and boundary conditions (u_i, i = 1 to 3, displacement in X_i direction).

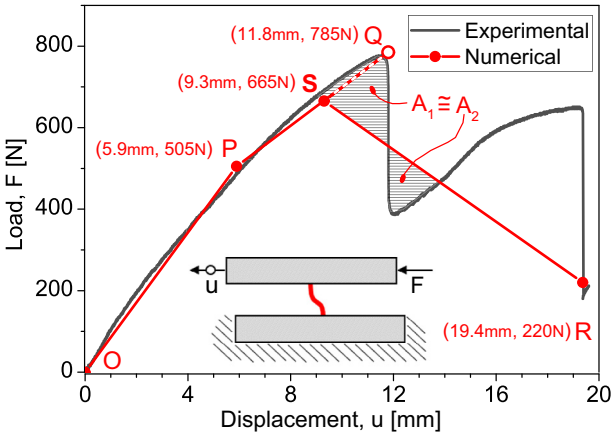

Fig. 21. Pushout test for assessing the stiffness contribution of the GFRP connector and the derived axial and shear stiffness.

1. The RSFRC exhibited satisfactory behaviour in terms of compressive strength and stress at crack initiation, and, more importantly, relatively high post-cracking tensile capacity. It has been shown that RSFRC is a viable solution for the production of facade panels to be applied in the structural (*e.g.*, seismic) rehabilitation of RC-frame buildings, as it allows for the production of thin laminar structural concrete elements, while contributing to a more sustainable construction sector.
2. The pushout tests performed for the selection of the type of insulation layer to be used in the sandwich panels showed that, although this component is regarded as being responsible almost exclusively for providing thermal insulation, it can afford non-negligible contribution to the structural performance of the panel. The experimental program revealed clear differences between specimens with different polystyrene typologies, therefore highlighting the influence of the adhesion between RSFRC and polystyrene on the overall structural performance of the sandwich panel solution under shear loading conditions. Specimens with XPS-3 core presented the highest in-plane shear capacity up to a relatively large lateral deformation (3 mm). EPS specimens, although having the lowest mechanical properties among all tested polystyrene typologies, performed better under shear loading when compared to the ones containing XPS with smooth surface finishing (XPS-5) – this result also stems from the different adhesion between the sandwich panel layers due to the polystyrene surface treatment.
3. The pushout tests where the diameter and anchorage depth of structural GFRP connectors was analysed showed that, for connectors with 8 mm of diameter, 35 mm of anchorage depth provided higher shear capacity due to the full mobilization of the connector's shear capacity. However, for the referred diameter, the specimens with 25 mm of anchorage depth presented higher ductility, indicating a better composite behaviour in terms of maximum lateral deformation (37 mm, + 48% compared to 35 mm of anchorage depth), while still ensuring a quite significant shear capacity. Regarding the connectors with 12 mm of diameter, better composite behaviour was obtained for specimens with the higher anchorage depth of 35 mm,

Table 6
Values adopted in the numerical simulation for the parameters of the IFE model.

Parameter	Value
Elastic stiffness in the orthogonal direction (k_n) [N/mm]	1.0
Elastic stiffness in the tangential directions (k_{t_1}=k_{t_2}) [N/mm]	1.0
Initial tensile strength ($f_{t,0}$) [MPa]	0.1
Initial cohesion for the cracking failure surface ($c_{0,F}$) [MPa]	0.11
Initial cohesion for the plastic potential function ($c_{0,P}$) [MPa]	0.025
Tangent of initial friction angle for the cracking failure surface ($\tan\phi_{0,F}$)[-]	0.37
Tangent of the initial friction angle for the potential function ($\tan\phi_{0,P}$) [-]	0.01
Tangent of the residual friction angle for the potential function ($\tan\phi_r$) [-]	0.001
Mode I fracture energy ($G_{F,I}$) [N/mm]	0.15
Mode II fracture energy ($G_{F,II}$) [N/mm]	0.20
Softening parameter for the tensile strength (λ_{f_t}) [-]	0.0
Softening parameter for the cohesion (λ_c) [-]	2.0
Softening parameter for the tangent of the friction angle ($\lambda_{\tan\phi}$) [-]	-1.0

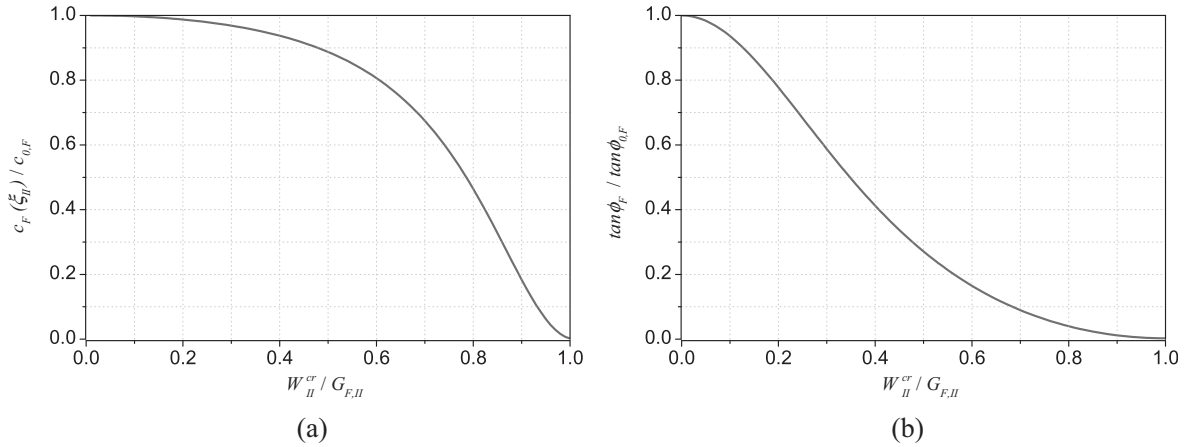

Fig. 22. Evolution of the parameters adopted in the numerical simulation (Table 6): (a) $c_F(\xi_{II})/c_{0,F}$ *vs.* $W^{cr}/G_{F,II}$; (b) $\tan\phi_F(\xi_{II})/\tan\phi_{0,F}$ *vs.* $W^{cr}/G_{F,II}$

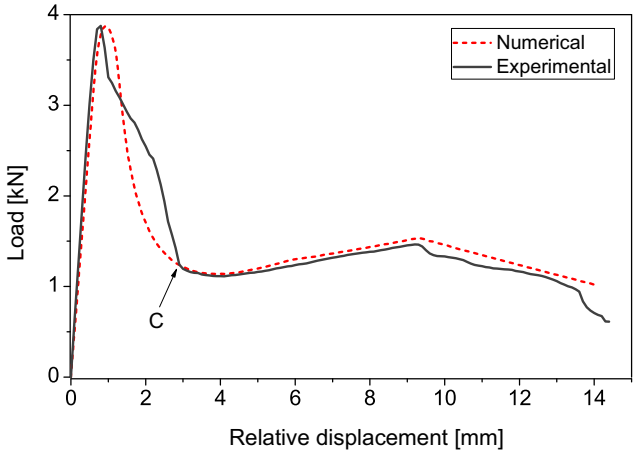

Fig. 23. Comparison between experimental and numerical results (for specimen typology FCØ10-H25-XPS3)

which provided a ductile behaviour and the highest load carrying capacity among all tested specimen typologies up to a lateral relative displacement of 24 mm. Overall, considering the proposed sandwich panel solution, the results obtained show that structural GFRP connectors with diameters of 8 and 12 mm are able to ensure the load transfer between RSFRC layers subjected to shear loading, especially when combined with anchorage depths of 25 and 35 mm, respectively; 12 mm diameter connectors are particularly well suited for applications with more demanding structural requirements.

4. The pullout tests showed a good bond behaviour between RSFRC and GFRP connectors, with the failure mode being governed by damage introduced in the surrounding RSFRC matrix, with average pullout loads higher than 9 kN for all tested configurations. The results of these tests also showed that the increase in anchorage capacity due to increasing RSFRC layer thickness seems to be more relevant for GFRP connectors with 12 mm of diameter.
5. Performed numerical simulations conducted to model the failure mechanisms observed at the interface between RSFRC and XPS-3 showed good agreement between experimental and numerical results. Based on the obtained results, the initial cohesion and friction angle between these materials is 110 kPa and 20°, with a softening evolution during the shear loading process, more pronounced in the friction angle.

The second part of the experiments aiming at the development of the sandwich panel included cyclic tests on RC frames strengthened with the sandwich panels and subjected to pseudo-dynamic cyclic loads. These recently completed tests, which will be presented in an upcoming publication, address the evaluation of the seismic performance of this sandwich panel reinforcement solution, namely in increasing the stiffness and strength of RC-frames under lateral loading.

CRediT authorship contribution statement

Christoph de Sousa: Conceptualization, Methodology, Investigation, Data curation, Formal analysis, Writing - original draft, Visualization. **Joaquim A.O. Barros:** Conceptualization, Methodology, Software, Validation, Formal analysis, Resources, Writing - review & editing, Supervision, Funding acquisition. **João Ramôa Correia:** Conceptualization, Methodology, Validation, Resources, Writing - review & editing, Supervision, Funding acquisition. **Tiago D.S. Valente:** Software, Writing - review & editing.

Declaration of Competing Interest

The authors declare that they have no known competing financial interests or personal relationships that could have appeared to influence the work reported in this paper.

Acknowledgements

The first author wishes to acknowledge the financial support provided by the Portuguese Foundation for Science and Technology (FCT) and the Eco-Construction and Rehabilitation (EcoCoRe) Doctoral Program through the research grant PD/BD/52657/2014. The second author acknowledges the support provided by the project ICoSyTec, POCI-01-0145-FEDER-027990, financed by the FCT (Portuguese Foundation for Science and Technology) and co-funded by FEDER through Operational Competitiveness and Internationalization Programme (POCI). The authors would like to thank the support and collaboration of the following companies: (i) *Twincon*, for supplying the RSF; (ii) *BVT-Rausch* and *PreConTech*, for supplying the F-GFRP connectors; (iii) *Schöck Bauteile GmbH*, for supplying the S-GFRP connectors; (iv) *Danosa/Eurofoam* and *Iberfibran*, for supplying polystyrene plates; and *S&P Clever Reinforcement*, for supplying the epoxy adhesive resin. The authors also wish to thank everyone that helped during the experimental work that was carried out in the Structural Laboratory from University of

Minho (LEST), at the CiviTest company and also at the Instituto Superior Técnico of Lisbon University.

References

[1] M.A. Kyriakides, Seismic retrofit of unreinforced masonry infills in non-ductile reinforced concrete frames using engineered cementitious composites [PhD Thesis]:, Stanford University, 2011.
[2] E. Esmaeeli, J.A.O. Barros, J. Sena-Cruz, H. Varum, J. Melo, Assessment of the efficiency of prefabricated hybrid composite plates (HCPs) for retrofitting of damaged interior RC beam–column joints, Compos. Struct. 119 (2015) 24–37.
[3] F. Akhoundi, Strategies for seismic strengthening of masonry infilled reinforced concrete frames [PhD Thesis], University of Minho, School of Engineering, Guimarães, Portugal, 2016.
[4] M.S. Hadi, T. Tran, Seismic rehabilitation of reinforced concrete beam–column joints by bonding with concrete covers and wrapping with FRP composites, Mater. Struct. 1–19 (2015).
[5] G.E. Thermou, V.K. Papanikolaou, A.J. Kappos, Flexural behaviour of reinforced concrete jacketed columns under reversed cyclic loading, Eng. Struct. 76 (2014) 270–282.
[6] J. Shin, J. Kim, K. Lee, Seismic assessment of damaged piloti-type RC building subjected to successive earthquakes, Earthquake Eng. Struct. Dyn. 43 (2014) 1603–1619.
[7] A.P.G. Martins, Seismic behaviour of masonry veneer walls [PhD Thesis]: University of Minho, School of, Engineering (2018).
[8] G. Martinopoulos, Life Cycle Assessment of solar energy conversion systems in energetic retrofitted buildings, Journal of Building Engineering. 20 (2018) 256–263.
[9] M.R. Heras, M.J. Jiménez, M.J.S. Isidro, L.F. Zarzalejo, M. Pérez, Energetic analysis of a passive solar design, incorporated in a courtyard after refurbishment, using an innovative cover component based in a sawtooth roof concept, Sol. Energy 78 (2005) 85–96.
[10] C.S.P. López, F. Frontini, Energy Efficiency and Renewable Solar Energy Integration in Heritage Historic Buildings, Energy Procedia 48 (2014) 1493–1502.
[11] European Commission. Directive 2018/2002 of the European Parliament and of the Council of 11 December 2018 amending Directive 2012/27/EU on energy efficiency. Official Journal of the European Union. 2018:210-29.
[12] European Commission. Directive 2018/410 of the European Parliament and of the Council of 14 March 2018 amending Directive 2003/87/EC to enhance cost-effective emission reductions and low-carbon investments, and Decision 2015/1814. Official Journal of the European Union. 2018:3-27.
[13] European Commission. Directive 2018/2001 of the European Parliament and of the Council of 11 December 2018 on the promotion of the use of energy from renewable sources. Official Journal of the European Union. 2018:82-209.
[14] R.F.W. Boarder, P.L. Owens, J.M. Khatib, The sustainability of lightweight aggregates manufactured from clay wastes for reducing the carbon footprint of structural and foundation concrete, Sustainability of Construction Materials (Second Edition): Woodhead Publishing, 2016, pp. 209–244.
[15] O. Kayali, Sustainability of fibre composite concrete construction, in: J.M. Khatib (Ed.), Sustainability of Construction Materials (Second Edition), 21, Woodhead Publishing, 2016, pp. 539–566.
[16] H. Savastano, S.F. Santos, J. Fiorelli, V. Agopyan, Sustainable use of vegetable fibres and particles in civil construction, in: J.M. Khatib (Ed.), Sustainability of Construction Materials (Second Edition), 19, Woodhead Publishing, 2016, pp. 477–520.
[17] F. Aslani, G. Ma, D.L. Yim Wan, G. Muselin, Development of high-performance self-compacting concrete using waste recycled concrete aggregates and rubber granules, J. Clean. Prod. 182 (2018) 553–566.
[18] L. Lourenço, Z. Zamanzadeh, J.A.O. Barros, M. Rezazadeh, Shear strengthening of RC beams with thin panels of mortar reinforced with recycled steel fibres, J. Clean. Prod. 194 (2018) 112–126.
[19] Z.T. Değer, T.Y. Yang, J.W. Wallace, J. Moehle, Seismic performance of reinforced concrete core wall buildings with and without moment resisting frames, The Structural Design of Tall and Special Buildings. 24 (2015) 477–490.
[20] RSA. Code for safety and actions for building and bridge structures (RSA) - Decree-Law n° 235/83 of May 31st (in Portuguese). Lisbon, Portugal1983.
[21] RCCTE. Regulation on the characteristics of the thermal performance of buildings (RCCTE) - Decree-Law 40/90 of February 6th (in Portuguese). Lisbon, Portugal1990.
[22] Pilakoutas K, Neocleous K, Tlemat H. Reuse of tyre steel fibres as concrete reinforcement. Proceedings of the ICE - Engineering Sustainability. 2004;157:131-8.
[23] A.M. Marques, J.R. Correia, J. de Brito, Post-fire residual mechanical properties of concrete made with recycled rubber aggregate, Fire Saf. J. 58 (2013) 49–57.
[24] M.A. Aiello, F. Leuzzi, G. Centonze, A. Maffezzoli, Use of steel fibres recovered from waste tyres as reinforcement in concrete: Pull-out behaviour, compressive and flexural strength, Waste Manage. 29 (2009) 1960–1970.
[25] A. Caggiano, P. Folino, C. Lima, E. Martinelli, M. Pepe, On the mechanical response of Hybrid Fiber Reinforced Concrete with Recycled and Industrial Steel Fibers, Constr. Build. Mater. 147 (2017) 286–295.
[26] G. Centonze, M. Leone, M.A. Aiello, Steel fibers from waste tires as reinforcement in concrete: A mechanical characterization, Constr. Build. Mater. 36 (2012) 46–57.
[27] Z. Zamanzadeh, L. Lourenço, J. Barros, Recycled Steel Fibre Reinforced Concrete failing in bending and in shear, Constr. Build. Mater. 85 (2015) 195–207.
[28] C. Frazão, Recycled Steel Fiber Reinforced Concrete for Structural elements subjected to chloride attack: Mechanical and Durability performance [PhD Thesis], School of Engineering of the University of Minho, Guimarães, Portugal, 2019.
[29] K.-B. Choi, W.-C. Choi, L. Feo, S.-J. Jang, H.-D. Yun, In-plane shear behavior of insulated precast concrete sandwich panels reinforced with corrugated GFRP shear connectors, Compos. B Eng. 79 (2015) 419–429.
[30] W. Choi, S.-J. Jang, H.-D. Yun, Design properties of insulated precast concrete sandwich panels with composite shear connectors, Compos. B Eng. 157 (2019) 36–42.
[31] B. Cox, P. Syndergaard, S. Al-Rubaye, F.F. Pozo-Lora, R. Tawadrous, M. Maguire, Lumped GFRP star connector system for partial composite action in insulated precast concrete sandwich panels, Compos. Struct. 229 (2019) 111465.
[32] M.J. Gombeda, C.J. Naito, S.E. Quiel, Development and performance of a ductile shear tie for precast concrete insulated wall panels, Journal of Building Engineering. 28 (2020) 101084.
[33] K. Hodicky, G. Sopal, S. Rizkalla, T. Hulin, H. Stang, Experimental and Numerical Investigation of the FRP Shear Mechanism for Concrete Sandwich Panels, J. Compos. Constr. 19 (2015) 04014083.
[34] J. Huang, Q. Jiang, X. Chong, X. Ye, D. Wang, Experimental study on precast concrete sandwich panel with cross-shaped GFRP connectors, Mag. Concr. Res. 72 (2020) 149–162.
[35] J.-Q. Huang, J.-G. Dai, Direct shear tests of glass fiber reinforced polymer connectors for use in precast concrete sandwich panels, Compos. Struct. 207 (2019) 136–147.
[36] Pahn M. GFRP-reinforcement bars as fasteners for high heat-insulating multi-layered sandwich panels. FRPRCS'11: 11th International Symposium on Fiber Reinforced Polymers for Reinforced Concrete Structures. Guimarães2013.
[37] D.G. Tomlinson, N. Teixeira, A. Fam, New Shear Connector Design for Insulated Concrete Sandwich Panels Using Basalt Fiber-Reinforced Polymer Bars, J. Compos. Constr. 20 (2016) 04016003.
[38] R. Lameiras, J. Barros, M. Azenha, I.B. Valente, Development of sandwich panels combining fibre reinforced concrete layers and fibre reinforced polymer connectors. Part II: Evaluation of mechanical behaviour, Compos. Struct. 105 (2013) 460–470.
[39] B.A. Frankl, G.W. Lucier, T.K. Hassan, S.H. Rizkalla, Behavior of precast, prestressed concrete sandwich wall panels reinforced with CFRP shear grid, PCI Journal. 56 (2011) 42–54.
[40] H. Hu, P. Papastergiou, H. Angelakopoulos, M. Guadagnini, K. Pilakoutas, Mechanical properties of SFRC using blended manufactured and recycled tyre steel fibres, Constr. Build. Mater. 163 (2018) 376–389.
[41] CEN. EN 12390-13. Testing hardened concrete - Part 13: Determination of secant modulus of elasticity in compression. 2013.
[42] CEN. EN 12390-3. Testing hardened concrete - Part 3: Compressive strength of specimens. 2009.
[43] Schneider Electronics. Inductive sensors XS4. Product data sheet XS4P12AB120. 2018. p. 7.
[44] Fédération Internationale du Béton. fib Model Code 2010 (final draft). fib, prepared by fib Special Activity Group 5, based on the draft published as fib Bulletins 55 and 56; 2011. p. 653.
[45] RIA-Polymers GmbH. RIALENE P 101 SGF50 ST natural. Technical Data Sheet. 2012.
[46] Schöck Bauteile GmbH. Schöck Combar® - Technical Information. 2015. p. 44.
[47] Danosa. DANOPREN FS-P 50. Technical data sheet (in Portuguese). 2018. p. 4.
[48] EPS - Empresa de Poliestireno Expandido L. EPS 100. Technical data sheet (in Portuguese). 2017. p. 1.
[49] fibran. fibranXPS ETICS GF. Technical Data Sheet. 2009. p. 2.
[50] Saari WK, Schultz AE, Hajjar JF, Shield CK. Behavior of shear connectors in steel frames with reinforced concrete infill walls. Structural Engineering Report No ST-99-1. Minneapolis, Minnesota: University of Minnesota - Institute of Technology. Department of Civil Engineering.; 1999. p. 189.
[51] Shim HB, Chung KS, Jang SH, Park SJ, Lee JH. Push-out tests on shear studs in high strength concrete. Fracture Mechanics of Concrete and Concrete Structures - Assessment, Durability, Monitoring and Retrofitting of Concrete Structures (FraMCos-7). Korea Concrete Institute, Seoul, South Korea2010.
[52] Wang W-l, Chen J, Jin W-l. Experimental Investigation of Corroded Stud Shear Connectors Subjected to Fatigue Loading. Journal of Materials in Civil Engineering. 2017;29:04016175.
[53] M. Flansbjer, D. Honfi, D. Vennetti, U. Mueller, N. Williams Portal, L. Wlasak, Structural performance of GFRP connectors in composite sandwich facade elements, J. Facade Des. Eng. 4 (2016) 35–52.
[54] S&P Clever Reinforcement. S&P Resin 55 - Epoxy adhesive (laminating resin). 2018.
[55] I.C. Rosa, J.P. Firmo, J.R. Correia, J.A.O. Barros, Bond behaviour of sand coated GFRP bars to concrete at elevated temperature – Definition of bond vs. slip relations, Compos. B Eng. 160 (2019) 329–340.
[56] Barros JAO. Debilities and strengths of FEM-based constitutive models for the material nonlinear analysis of steel fiber reinforced concrete structures. In:

Saouma V, Bolander J, Landis E, editors. 9th International Conference on Fracture Mechanics of Concrete and Concrete Structures - FraMCoS-9. California2016
[57] A. Caballero, K.J. Willam, I. Carol, Consistent tangent formulation for 3D interface modeling of cracking/fracture in quasi-brittle materials, Comput. Methods Appl. Mech. Eng. 197 (2008) 2804–2822.
[58] M. Coelho, Bond behaviour of NSM FRP systems in concrete [PhD Thesis], University of Minho, Guimarães, Portugal, 2016.
[59] A.M. Papadopoulos, State of the art in thermal insulation materials and aims for future developments, Energy Build. 37 (2005) 77–86.
[60] F. Müller, Sandwichelemente mit Deckschichten aus Hochleistungsbeton und einem Kern aus extrudiertem Polystyrol [PhD Thesis], Technischen Universität Kaiserslautern (2015).
[61] D. Figueira, J. Sena-Cruz, E. Pereira, I. Valente, J. Barros, F. Castro, et al., Influence of service temperature on shear creep behaviour of a rigid low-density closed-cell PIR foam, Constr. Build. Mater. 225 (2019) 1052–1063.